PERFORMANCE EVALUATION OF A TWO-BAR BRIDGE RAIL FOR COMPLIANCE WITH MASH TL-3 CONDITIONS USING FINITE ELEMENT ANALYSIS

by

Joshua Fatoki

A thesis submitted to the faculty of
The University of North Carolina at Charlotte
in partial fulfillment of the requirements
for the degree of Master of Science in
Mechanical Engineering

Charlotte

2020

Approved by:

_____
Dr. Howie Fang

_____
Dr. Alireza Tabarraei

_____
Dr. David C. Weggel

ABSTRACT

JOSHUA FATOKI. Performance evaluation of a two-bar bridge rail for compliance with MASH TL-3 conditions using finite element analysis. (Under the direction of DR. HOWIE FANG)

Roadside barriers are important safety devices installed on highways to mitigate the severity of injuries caused by crashes of errant vehicles. The two-bar metal bridge rail is a commonly used roadside barrier in North Carolina and is recognized for its performance and aesthetics. Currently, all safety devices used on U.S. highways must be tested to meet the safety criteria specified by the Manual for Assessing Safety Hardware (MASH). This thesis presents the research using finite element (FE) modeling and simulations to evaluate the performance of a two-bar bridge rail for its compliance with MASH TL-3 requirements. The modeling and simulation work were conducted on the two-bar bridge rail under vehicular crashes of a 2010 Toyota Yaris, a 2007 Chevy Silverado, and a 2014 Chevy Silverado at a speed of 62 mph (100 km/hr.) and at a 25° angle. The MASH evaluation criteria *A*, *D*, *F*, and *H* were used to access the impact performance of the bridge rail. In addition, the simulation results were compared to test data of vehicles impacting the bridge rail under the same impact conditions. The simulation results showed that under MASH TL-3 conditions, the bridge rail could safely contain and redirect the test vehicles. Furthermore, the simulation results were shown to generally agree well to the actual test data and satisfied the MASH evaluation criteria.

ACKNOWLEDGEMENTS

I must begin by expressing my sincere gratitude to my advisor, Dr. Howie Fang, for giving me the opportunity to work in his research lab during my undergraduate and graduate studies. His support, guidance, knowledge and mentorship have helped me a great deal than I could ever give him credit for here. I would also like to thank my committee members, Dr. Alireza Tabarraei and Dr. David Weggel, for their valuable reviews, comments, and advice on my thesis.

I am especially indebted to the North Carolina Department of Transportation (NCDOT) for their financial support to me as a research assistant in the NCDOT Project 2019-23. I would also like to thank my research colleagues: Zheng Li, Emre Palta, and Lukasz Pachocki for their indispensable help and advice during my research work.

Most importantly, I wish to thank my family, friends, and especially Chiamaka Azih for their encouragement, love and support during my graduate studies.

TABLE OF CONTENTS

LIST OF TABLES

LIST OF FIGURES

CHAPTER 1: INTRODUCTION

Roadside barriers are important safety devices installed on highways to mitigate the severity of injuries caused by crashes of errant vehicles, e.g., containing and redirecting errant vehicles by longitudinal barriers such as a bridge rail system. The NCDOT two-bar metal bridge rail, as shown in Fig. 1.1, is a frequently used longitudinal barrier on bridges in North Carolina and is recognized for its performance and aesthetics. Currently, all safety devices used on U.S. highways must be tested to meet the safety criteria specified by the Manual for Assessing Safety Hardware (MASH) issued by the American Association of State Highway and Transportation Officials (AASHTO). While full-scale crash testing is a valid means of evaluating the safety performance of bridge rails, it is very expensive, time-consuming, and difficult to perform. With the rapid development of computing hardware and commercial software for high performance computing, computer simulations have been increasingly used to evaluate the performance of roadside safety barriers. In this section, an extensive summary of studies related to bridge rails and the application of finite element (FE) analysis on their safety performance are provided.

Figure 1.1: An NCDOT Two-bar bridge rail.

1.1 Performance Evaluation of Bridge Rail Barriers

Since the creation of *Standard Specifications for Highway Bridges and Incidental Structures* by AASHTO in 1931, bridges have been required to follow design specifications. Prior to 1953, performance evaluation of bridge rails was primarily conducted onsite after a vehicle collision occurred. In 1955, the state of California pioneered several dynamic full-scale impact tests of bridge rail systems as an alternative for onsite evaluation of the impact performance of bridge rails. During these tests, it was observed that there was an extremely high probability of vehicle snagging in the existing baluster-type rail designs. Consequently, the baluster-type rail designs were replaced by the solid, non-yielding smooth-wall barriers that were deemed more effective. Furthermore, as a result of these impact tests, the Type 1 bridge rail design was adopted by the California Division of Highways. The Type 1 bridge rail utilized an extruded metal rail and posts mounted on a reinforced concrete parapet.

In the early 1960s, Nordlin et al. (1965) evaluated the impact performance of three different bridge rail designs, a standard California Type 1, a standard California Type 2, and an experimentally modified Type 1 bridge rail. Five full-scale crash tests were conducted to evaluate the overall effectiveness and structural adequacy of the bridge rail designs. The designs of the three bridge rails were evaluated based on four criteria: the ability to retain the vehicle on the structure, structural integrity of the bridge rail after an impact, potential of vehicle snagging, and ease of repair. The results of these full-scale crash tests led to several significant conclusions on the performance of bridge rail systems. Although all four evaluation criteria were met, it was observed that the test vehicles exhibited various post-impact behaviors for different barrier heights. For instance, there

was no tendency for the test vehicle to climb the barrier when the parapet was sufficiently high to absorb a significant portion of the impact energy. However, severe deformations on the body and frame of the test vehicles were observed at these elevated barrier heights. In addition, the test results indicated that when a significant portion of the impact load was taken by the metal rail, the rail deflections were excessive, and the vehicle almost vaulted over the rail. It was concluded that the modified Type 1 bridge rail with a 28-in high parapet (36-in. overall barrier height) was the most effective design among the three tested bridge rails.

An analysis performed in the late 1960s indicated that the New Jersey concrete median barrier mitigated the severity of deformations sustained by an errant vehicle because of its lower slope. Consequently, the Bridge Department of the California Division of Highways designed a bridge rail that incorporated the New Jersey type parapet and the tubular steel rails used in the California Type 1 bridge rail design (Nordlin et al., 1970). This new design was named the California Type 20 bridge rail and was evaluated using full-scale crash tests to determine its ability to safely redirect a vehicle and minimize deformations sustained by a vehicle during a collision. Analysis of the test results indicated that the sloped lower face of the parapet minimized the collision severity. However, the Type 20 bridge rail had limited see-through properties when compared to older designs.

Michie et al. (1981) conducted a research funded by the National Cooperative Highway Research Program (NCHRP) and published NCHRP Report 230 to provide guidelines for the safety evaluation of highway appurtenances. In 1986, FHWA issued a policy memorandum requiring bridge railings installed on federal interstates and state highways to meet or exceed the full-scale crash-test criteria of NCHRP Report 230 in order

to receive federal funding. Ross et al. (1993) published their results in NCHRP Report 350, which was adopted by researchers in the field to replace NCHRP Report 230. NCHRP Report 350 differed from NCHRP Report 230 in that it defined six test levels for rating the crashworthiness of highway barriers including bridge rails and specified a passenger sedan and a pickup truck as the standard test vehicles. It also provided guidelines for selecting the critical impact point for crash tests on redirecting-type safety hardware. NCHRP Report 350 provided information on enhanced measurement techniques related to occupant risk and reflected a critical review of methods and technologies for safety performance evaluation. Periodically, FHWA published lists of bridge rails considered crashworthy after being successfully crash tested. In 1997, FHWA issued a memorandum summarizing 68 crash-tested bridge rails and established the tentative equivalency of previous test level ratings for bridge rails in comparison to NCHRP Report 350, as summarized in Table 1. As shown in Table 1.1, test level 2 (TL-2) of the NCHRP Report 350, multiple service levels 1 and 2 (MSL-1 and MSL-2) of the NCHRP Report 230 and performance level 1 (PL-1) of the AASHTO Specifications for Bridge Railings are equivalent. The accepted equivalencies for NCHRP Report 350 test level 4 (TL-4) are also shown. The test levels of the bridge rail testing criteria shown in Table 1.1 varied by the recommended impact testing conditions: vehicle classification, impact speed and impact angle.

Table 1.1: Bridge rail test level equivalencies.

Bridge Rail Testing Criteria	**Acceptance Equivalencies**					
NCHRP Report 350	TL-1	TL-2	TL-3	TL-4	TL-5	TL-6
NCHRP Report 230		MSL-1 MSL-2		MSL-3		
AASHTO Guide Specifications for Bridge Railings		PL-1		PL-2	PL-3	
AASHTO LRFD Bridge Specifications		PL-1		PL-2	PL-3	

In 1997, an additional FHWA memorandum was published, requiring all highway safety hardware installed on or after October 1, 1998 to be crash tested and be in compliance with NCHRP Report 350. This memorandum allowed exceptions on some bridge rails tested and found acceptable for use on the National Highway System. In 2000, transportation agencies could request FHWA approval from state-specific bridge railings without full-scale testing but in compliance with NCHRP Report 350 requirements, provide an in-depth structural analysis of all possible failure modes and assumed behavior of all rail elements and connections. In addition to the structural analysis, bridge railings were required to also meet the dimensional and design requirements by the AASTHO LRFD Bridge Specifications. The impact conditions for test levels 1 to 4 in NCHRP Report 350 is shown in Table 1.2.

Table 1.2: NCHRP Report 350 impact conditions for test levels 1, 2, 3 and 4.

Test level	**Impact Conditions**		
	Vehicle (Mass)	**Speed (km/h)**	**Angle**
TL-1	Passenger car (820 kg) Pick-up Truck (2000 kg)	50 50	20° 25°
TL-2	Passenger car (820 kg) Pick-up Truck (2000 kg)	70 70	20° 25°
TL-3	Passenger car (820 kg) Pick-up Truck (2000 kg)	100 100	20° 25°
TL-4	Passenger car (820 kg) Pick-up Truck (2000 kg) Single Unit Truck (8000 kg)	100 100 80	20° 25° 15°

Bridge rails are usually attached to concrete decks. To evaluate the performance of bridge rails on bridge decks with different materials, Faller et al. (2000) investigated the crashworthiness of railing systems constructed on transverse timber decks. In this work, two bridge rails and approach guardrail transition systems for use on timber deck bridges were developed. The first bridge rail was constructed with glulam timber components, whereas the second one was built with steel hardware. The bridge rail was crash tested under NCHRP Report 350 TL-4 impact conditions. It was concluded from crash test results that the bridge rails and transition systems met the TL-4 requirements of NCHRP Report

350. In addition, the test results indicated that bridge rails constructed on timber decks would have similar performance to those constructed on concrete decks.

In 2001, the Texas Department of Transportation (TxDOT) contracted with the Texas Transportation Institute (TTI) to develop two crashworthy and aesthetically pleasing bridge rails for use on selected bridges and roadways. Several designs were conceptualized as a result of this work. The two final designs chosen were the Texas Type T-77 and F411 aesthetic bridge rails. The Texas Type F411 is a concrete bridge rail consisting of two six-inch (152-mm) wide concrete rails atop a 42 inches high parapet. Vertical reinforcements were incorporated into the concrete rails and parapet to increase the tensile strength. The parapet was secured to the bridge deck utilizing "U" Bars. The total height of the bridge rail is 42 inches (1.1 m). The second design, the T-77 bridge rail, consisted of two elliptical-shaped steel rails welded to steel posts. The posts and rails were anchored to a sloping-top steel curb. The total height of the T-77 bridge rail was 33 inches (0.8 m). The two designs were crash tested in accordance with the NCHRP Report 350 TL-3 impact conditions (Bullard et al., 2002). The Texas F411 design was shown to meet the evaluation criteria of NCHRP Report 350 for TL-3. However, the test results also indicated a potential for an errant vehicle to intrude into adjacent traffic lanes after a collision. The second aesthetic bridge rail developed, the Texas T-77, met the evaluation criteria of NCHRP Report 350 for Test 3-10 (i.e., impacted by the passenger car), but failed to pass the evaluation criteria for Test 3-11 (i.e., impacted by the pickup truck) due to the vehicle snagging at a rail splice joint and consequently causing excessive deformations of the occupant compartment.

To mitigate the cost associated with the construction and repair of aesthetic bridge rails, the Texas DOT sponsored another project to design, develop, and crash test a cost-

effective aesthetic and crashworthy bridge rail that would meet the TL-3 requirements of NCHRP Report 350. As a result of this work, Williams et al. (2008) designed the Texas Type T-1F bridge rail with aesthetic features and ease of constructing. The elliptical-shaped steel rails of the bridge rail were mechanically attached to the posts without welding and could be adjusted after installation, thereby making the bridge rail easier to construct and repair. The Texas Type T-1F bridge rail was crash tested to evaluate its compliance with the requirements of NCHRP Report 350. Performance evaluation of the bridge rail showed that the T-1F design met the TL-3 requirements of NCHRP Report 350. Even though the T-1F bridge rail demonstrated a potential for wheel snagging on rail splices, the lower yield strength of the aluminum rail and posts prevented excessive vehicular snagging and thus greatly reduced the deformations inside the vehicle compartment.

In the late 1990s, California DOT funded a project to develop and crash test two bridge rail designs, Type 80 and Type 80SW, for use on scenic highways. Both designs were made of concrete that incorporated a continuous square railing between the two end posts of the bridge. Analysis of the crash test results for these designs showed that Type 80 and Type 80SW met the TL-4 requirements of NCHRP Report 350. However, these designs had limited “see through” capabilities and exhibited a potential for vehicle snagging.

In a subsequent project also funded by the California DOT, an aesthetic one-bar bridge rail, Type 90, was designed to replace the previous Type 80 and Type 80SW bridge rails (Whitesel et al., 2008). The Type 90 design had adequate “see through” capabilities and required low maintenance. In this bridge rail design, a steel post and beam system is connected to a concrete parapet by anchor bolts. The steel railing consists of steel beams

securely attached to steel posts spaced three meters (3 m) apart. The newly designed Type 90 bridge rail was tested for compliance with NCHRP report 350. Three crash tests were carried out at the TL-4 levels of NCHRP Report 350. The test vehicles included an 820-kg small car, a 2000-kg pickup truck, and an 8000-kg single unit truck. The test results showed that there was minimal lateral deflection and negligible permanent damage to the concrete parapet. The barrier successfully contained and redirected the three test vehicles. More importantly, the results showed that the structural adequacy, vehicle trajectory as well as occupant safety criteria were within the acceptable limits outlined in NCHRP report 350.

In 2009, AASHTO published the Manual for Accessing Safety Hardware (MASH), which updated and superseded NCHRP Report 350 for evaluating new safety hardware devices. AASHTO and FHWA jointly adopted an implementation plan for MASH that all highway safety hardware accepted prior to the adoption of MASH – using criteria contained in NCHRP Report 350 – could remain in use and continue to be manufactured and installed. In addition, highway safety hardware accepted using NCHRP Report 350 criteria is not required to be retested using MASH criteria. However, new highway safety hardware not previously evaluated must be tested and evaluated using MASH. MASH represents an update to crash testing requirements based primarily on changes in the test vehicles.

William et al. (2013) conducted full-scale crash tests at MASH TL-3 conditions to evaluate the performance of a transition design for the Texas DOT T131RC bridge rail design. The performance of the bridge rail under impact was evaluated based on structural adequacy, occupant risk, and post-impact vehicle trajectories. Each test vehicle was instrumented with data acquisition system to measure accelerations and rotations (yaw,

pitch and roll). According to the test results, the T131RC bridge rail met the strength and safety performance criteria at MASH TL-3 conditions. In another work by William et al. (2015), a low-cost bridge rail system was designed that would minimize or eliminate bridge deck damage (observed from crash testing of prior designs) when impacted by errant vehicles. The newly developed bridge rail design was named the Texas Type T631 bridge rail. The Texas Type T631 consisted of W-beam rails securely bolted to steel posts that were welded to steel base plates. Crash testing was conducted to evaluate the bridge rail's compliance with MASH and was found to perform exceptionally well at TL-2 conditions. Subsequently, the Texas Type T163 bridge rail was revised with reduced post spacing (from 75 inches to 37½ inches) and was evaluated at MASH TL-3 conditions. The test results showed that the bridge rail with reduced post spacing met the MASH TL-3 requirements.

Over the years, the Type 26 bridge rails had been used on several bridges in California. To ensure its compliance with the requirements set by the FHWA, a project was initiated in the early 2000s to test the Type 26 bridge rail under TL-3 conditions of NCHRP report 350. The project, however, failed to meet the FHWA's deadline for NCHRP Report 350 testing.

The Type 26 bridge rail was subsequently redesigned to ensure it can be tested according to the MASH 09 guideline (Feinsod et al., 2016). The redesigned version was named Type 732SW, which was taller and stronger than the Type 26 bridge rail. The Type 732SW bridge rail system included a concrete parapet, steel handrails for pedestrian, and a sidewalk. Crash tests were conducted to evaluate the compliance of Type 732SW bridge rail to the MASH 09 requirements. The tests included Test 3-11 (i.e., using a 2270P pickup

truck) and Test 3-10 (i.e., using a 1100C passenger car). It was concluded that the Type 732SW bridge rail met all the requirements of MASH 09 for Test 3-11, but failed to meet the Occupant Risk criteria of MASH for Test 3-10. Analysis of the Test 3-10 results showed that the ridedown acceleration was too high, because the initial impact between the tire and the sidewalk edge was significant enough to reduce the lateral flail space before impacting the concrete parapet and caused the theoretical occupant impact to occur sooner than that for a narrower sidewalk. Because Type 732SW bride rail failed to meet the Occupant Risk criteria for Test 3-10, it was subsequently crash tested using Test 2-10, i.e., impacted by a 1100C passenger car at TL-2 conditions. The test results showed that the Type 732SW bridge rail met the requirements of MASH 09 for Test 2-10 and thus was recommended for approval on California highways requiring TL-2 bridge rails with pedestrian traffic.

Recently, AASHTO released the second version of MASH, i.e., MASH 2016, which ended the approval of roadside safety hardware compliant with NCHRP Report 350. In addition, AASHTO and FHWA issued a Joint Implementation Agreement that required all previously approved NCHRP Report 350 hardware installed on the National Highway System be replaced or retested to meet the MASH 2016 evaluation criteria. As a response to the AASHTO/FHWA Joint Implementation Agreement for MASH 2016, NCDOT outlined an implementation plan for the compliance of roadside safety hardware with MASH 2016 requirements.

1.2 Crash Modeling and Simulations

Historically, the safety performance of vehicles and roadside safety devices were evaluated through full-scale crash testing. While it is a valid means for evaluating the safety

performance of vehicles and roadway structures, physical crash testing is very expensive, time-consuming, and difficult to perform. Consequently, only a limited number of representative crash scenarios can be evaluated based on regulations given by MASH for roadside safety hardware designs. With the rapid development of computing hardware and commercial software for high performance computing, computer simulations have been increasingly used in highway safety designs. Full-scale FE simulations have been widely accepted as a powerful means to investigate various roadside safety issues. Compared to full-scale crash testing, FE simulations are particularly useful in assessing the performance of roadside structures under various impact and site conditions that would be either impossible or impractical for conducting physical experiments. In recent decades, various FE models of vehicles and roadside safety devices have been developed.

Wekezer et al. (1993) developed the first FE model for vehicle-roadside hardware impact simulations. Prior to this, simulations of vehicle-roadside hardware impacts were only performed using some deformable parts of a vehicle and a rigid part representing the safety hardware. This research was one of several projects funded by FHWA with the aim of developing better FE models that could predict vehicle and barrier responses during impacts. In this research, a simple FE model of a 1991 GM Saturn was developed to demonstrate FE modeling capabilities for crash simulations. Two impact scenarios were examined: the vehicle impacting a rigid wall and impacting a luminaire pole. The simulation results were compared with crash test data performed by the National Highway Traffic Safety Administration (NHTSA). The simulation results were found to match well to test data and the FE modeling technique was shown to be effective in predicting vehicular responses in impacts. In a similar project also funded by FHWA, Mendis et al.

(1995) developed an FE model of a 1981 Honda Civic to evaluate the crash performance in a frontal impact with a highway sign posts and barriers. Because the scope of this research was limited to frontal impact conditions, the rear half of the vehicle was assumed to be rigid and only the front half was modeled as deformable parts. The simulation results were compared with test data from a previous crash test. The comparison showed that the deformation pattern predicted by the FE simulation was similar to those observed in the actual crash test. Although the overall response of the FE model was considered to be satisfactory, this model was limited to frontal impacts of the vehicle with narrow object and rigid walls.

Cofie et al. (1995), developed a simple FE model of a 1989 Ford Festiva, with improvements over some of the limitations observed in previous vehicle models. For instance, an accelerometer model was incorporated in this FE model at the center of gravity of the vehicle. Consequently, the vehicle's accelerations, velocities and displacements could be obtained from simulations and compared directly with actual test data. The test conditions used in this study were frontal impacts and the simulation results were shown to agree with the actual test results.

Over the years, NHTSA and FHWA funded several projects on the development of FE models that could be used in roadside safety research to gain better knowledge of highway/vehicle safety issues and to assist mitigating the severity of highway crashes. In one of these projects, researchers at George Washington University developed the FE model of a 1994 Chevrolet C-1500 pick-up truck for roadside hardware impact simulations (Zaouk et al., 1997). Since previous vehicle models were developed for only frontal impacts, the accuracy of simulation results obtained using these models for other impact

conditions were questionable. The C-1500 was the first FE model developed for both frontal and side impact scenarios. The approach taken by the researchers involved creating a detailed and a simplified vehicle model. The simplified model was used to test various components of the detailed model. In addition, tensile and shear tests were conducted on several components of the vehicle such as the fender, bumper and door frames to obtain their material properties. Two crash tests, a frontal impact with a rigid wall and a side impact with a vertical concrete barrier, were used to validate the vehicle models. It was shown that the vehicle trajectory from the simulation results was similar to that from the actual test. In addition, the deformations observed from frontal and side impact simulations agreed with test results. It was concluded that the simulation results had good agreement with test data for the various levels of comparison. The researchers also suggested that it was necessary to further improvement to the models' fidelity.

FE simulations have been increasingly used to determine if a safety barrier would pass the requirements of safety guidelines before conducting full-scale crash tests. Ray et al. (2004) used FE simulations to design and analyze a newly developed aluminum F-shape bridge railing. The objective of the research was to assess the barrier's performance under the TL-3 and TL-4 conditions of NCHRP Report 350. The FE model of a C2500 pickup truck, which included fully functioning suspension, steering and tire models, was used in the simulation of impacting the aluminum F-shape bridge rail at TL-3 condition. The FE model of an 800S single-unit truck was used in the simulation of the TL-4 test. The simulation results showed that the bridge rail mainly remained intact, with only minor deformations and reasonable local deformations at both test levels. Furthermore, the FE simulation results were shown to have good agreement with the crash test data on the

predicted characteristics and crash responses of the bridge rail. It was concluded that the bridge rail's performance was acceptable under TL-3 and TL-4 conditions of NCHRP Report 350.

In the work by William et al. (2008), FE analysis was utilized in the design of the Texas T-1F bridge rail, specifically to determine the overall stiffness, thickness and ultimate force that could be applied to the proposed T-1F posts and ultimately to the 7⁄8-in. diameter anchor bolts. In addition, FE analysis was used to investigate several failure modes in the posts due to impact loading. Based on the analysis, the thickness of the posts and base plates were determined. Subsequent simulation results showed that the proposed bridge rail design met the minimum strength requirement of the AASHTO LRFD TL-3 loading conditions.

In recent years, there have been a considerable amount of work done on the validation of several components of publicly available vehicle models. In the first phase of their study, Mohan et al. (2009[a]) conducted several full-scale tests to generate data that would be used to validate the steering and suspension system of the FE model of a 2007 Chevrolet Silverado pick-up truck that was being developed. In the first series of tests, low-speed non-destructive tests were conducted to measure suspension deflections when the vehicle went through speed bumps and sloped terrains. In the second series of tests, the front and rear suspensions were subjected to vertical and lateral loading from a swinging rigid pendulum. In the second phase of the study, Mohan et al. (2009[b]) developed a FE model of a 2007 Chevrolet Silverado pick-up truck. The detailed model incorporated every structural part of the physical vehicle and reflected the functionality of the steering and suspension systems. The accuracy of this model was accessed for several impact scenarios.

These included frontal impact into a rigid wall, centerline pole impact, and side impacts at varying speeds. Subsequently, the results were validated with actual data from the preceding crash tests. The vehicles response and damage profile were consistent with actual data for all impact conditions investigated. It was concluded that the FE model is suitable the for various impact conditions and satisfies the requirements for a 2270P test vehicle under the crashworthiness evaluation criteria specified in MASH.

Fang et al. (2009) used FE analysis to evaluate two retrofit options to enhance the performance of cable median barriers (CMBs). In their work, several CMB designs for each retrofit option were evaluated using full-scale FE simulations of a vehicle crashing into a cable median barrier. The safety performance of these retrofit designs was evaluated for both front-side and back-side impacts at different impact speeds and angles. The simulation results showed that some retrofit options could enhance the CMB performance for back-side impacts without compromising the performance for front-side impacts.

In the work by Marzougui et al. (2011), they developed an FE model of a 2010 Toyota Yaris passenger sedan. This vehicle was selected for modeling to reflect the automotive designs and technology advancements at the time for an important segment of the vehicle fleet. In addition, it conforms to the MASH requirements for 1100C test vehicles. Similar to the 2007 Chevrolet Silverado, the Toyota Yaris model incorporated a functional suspension and steering subsystems. The model was subsequently validated against actual crash test data from NHTSA on the corresponding vehicle. It was concluded that the overall responses of the vehicle from simulation results were consistent with those from the actual test data. Furthermore, both the vehicle kinematics and accelerometer

output data from simulations were shown to have a good correlation with the physical test data.

A commercial FE program, LS-DYNA, is widely used in analysis of impact responses of various structures. Much work has been done over the years since its pioneer version to improve the FE program's capability to accurately simulate vehicular impacts. Abu-Odeh (2006[a]) evaluated the suitability of three concrete material models in LS-DYNA, i.e., material types 72R3, 84 and 159, for modeling the deformations and damages of concrete barriers under impact loading. Furthermore, the research focused on providing analysts methods of modeling concrete materials with minimum user inputs. To compare the damages of a concrete barrier predicted by the material models with actual test data, a Texas F-shaped barrier (TxDOT T501) was used in the simulation of impacts by a 5000-lb bogie. The simulation results showed that all three material models performed reasonably well. It was also suggested that the accuracy of these models could be improved by calibrating the models' input parameters.

In another study by Abu-Odeh (2006[b]), the FE model of a Texas T4 bridge rail was created to evaluate the suitability of LS-DYNA concrete material model, MAT 159, for analyzing concrete roadside safety features. MAT 159 has two formats: MAT_CSCM (short input format that utilizes hard-coded default values for numerous variables), and MAT_CSCM_CONCRETE (long input format for which the user must supply values for all the required input parameters). The T4 bridge rail consisted of steel elliptical rails, posts, and base plates attached to a reinforced concrete parapet. The study was intended to evaluate the capability of the material model in capturing concrete deformations. In addition, MAT_CSCM, was compared with MAT_CSCM_CONCRETE to determine the

better one in capturing concrete damage. A sensitivity study was performed on MAT_CSCM_CONCRETE model to evaluate the parapet's response to different combinations of the required parameter inputs. Finite element simulations were also conducted on the concrete barrier impacted by two different pendulums. The simulation results showed that MAT_CSCM_CONCRETE could capture the deformation patterns observed in the actual test and thus was deemed better than MAT_CSCM. Furthermore, it was concluded that MAT_CSCM_CONCRETE was suitable for modeling concrete bridge rails.

Several methods have been reported in literature to address the issue of modeling steel reinforcements in concrete materials using FE analysis. Schewer (2014) evaluated three methods of modeling rebars in reinforced concrete slabs. The first approach involved homogenizing the material properties of the concrete and rebar by combining the volume-fraction ratio of the steel and concrete materials. This approach for modeling reinforced concrete is commonly known as the smeared reinforcement. The second method evaluated by Schewer to model reinforced concrete, known as the constraint method, was to couple the rebars with the surrounding concrete continuum using an internally generated constraint in LS-DYNA. The third method, also known as the shared-nodes method, involved constructing the mesh in such a way that the nodes of the reinforcement grid were coincident with the nodes on the mesh of the surrounding concrete. The performance of these methods of modeling rebars in reinforced concrete slabs was evaluated under three loading conditions. The loading conditions include axial extension, self-weight and blast loading. Simulation results showed that under axial extension loading, the constraint method was unable to predict the effect of the steel reinforcement in the concrete because

the deformation profile of the concrete was like the case with no rebar. For the self-weight loading condition, the smeared reinforcement technique failed to accurately predict the deflection of the concrete. As a result, it was concluded that smeared reinforcement technique is only suited for small displacement when the reinforcement remains elastic. Results from the final loading condition (blast loading) showed that the shared nodes and constraint methods were able to predict the displacement of the concrete. Conversely, the smeared reinforcement approach failed to accurate represent the reinforcement in the concrete or predict the deflection of the concrete. In fact, the entire concrete slab failed catastrophically. Only the shared node approach of modeling reinforced concrete performed well in all three loading conditions.

There is a considerable amount of literature on FE modeling techniques for bolted joint representations in crash simulations. Narkhede et al. (2010) examined two approaches for representing bolted joints in LS-DYNA to model bolt pre-stresses and bolt failure characteristics in crash simulations. The first approach involved modeling the bolt shank with beam elements and modeling its connection to surrounding plate with discrete spring elements. In addition, the bolt head and nut were modeled using rigid shells. In the second approach, the bolt shank, bolt head and nut were modeled using solid elements. The bolt responses were compared to analytical solutions for shear, compressive and tensile loading conditions. It was concluded that the bolted joint responses predicted by the two modeling techniques were shown to have a good agreement with analytical solutions as well as physical test data under shear and tensile loading conditions.

In a research sponsored by the United States Marine Corps, Hadjioannou et al. (2016) investigated different approaches for modeling bolted connections using both

numerical simulations and physical experiments. The study focused on developing computationally efficient methods to represent bolted joints under static and dynamic loading conditions. Simplified FE models of bolted connections were developed utilizing a combination of beam and shell elements. The simulation results of the simplified model were compared to static and dynamic test data. It was concluded that the simplified model could simulate the behavior of bolted connections with reasonable accuracy.

In the remaining chapters of this thesis, details of the full-scale crash simulations on the bridge rail using detailed FE models of a 2010 Toyota Yaris, a 2007 Chevy Silverado, and a 2014 Chevy Silverado are discussed. Also, a brief description of how contact between interacting components was modeled is provided. Test data from full-scale crash tests of the NCDOT two-bar bridge rail conducted by MwRSF was used to validate the FE model. In addition, results from the FE simulation were used to evaluate the impact performance of the bridge rail.

CHAPTER 2: CONTACT THEORY AND METHODS

Modeling interface interactions is crucial when applying finite element methods to solve engineering impact problems. Over the years, different methods and algorithms have been developed to solve complicated contact problems. The contact modeling process typically commences by searching for penetrations at every time step. If a penetration is detected, the contact boundary conditions are enforced to remove the penetrations using user-specified contact algorithms. The most commonly used algorithms for enforcing contact boundary conditions are based on the Lagrange multiplier method, augmented Lagrangian method or the penalty method. In LS-DYNA, contact boundary conditions can be enforced using the kinematic constraint method, the penalty method or the distributed parameter approach. Detailed descriptions of contact theory and application of the various contact handling methods can be found in Wriggers (2016). A brief description of the penalty method, which was mostly used in this work, is given in this chapter.

2.1 Penalty-based Methods

In penalty-based methods, contact boundary conditions are enforced by applying a resisting force (also called contact force) to each of the two interacting bodies so as to separate them and

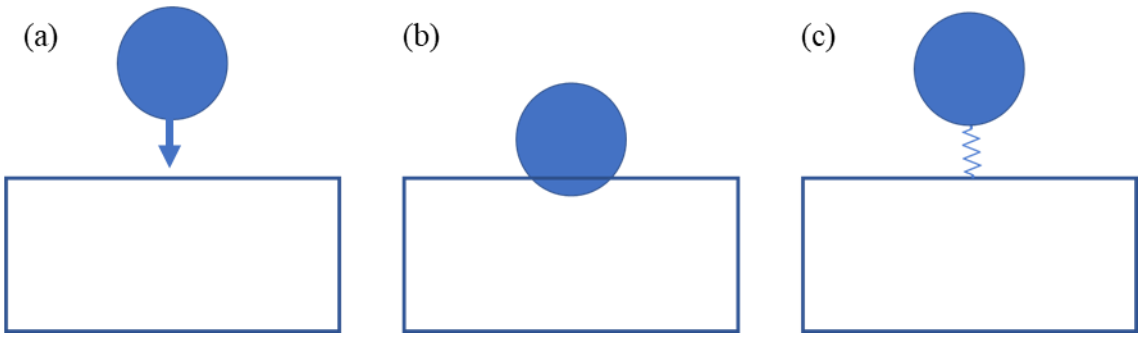

Figure 2.1: (a) Impactor approaches object. (b) The impactor penetrates the object. (c) Impactor supported by a penalty spring (with a contact stiffness).

eliminate penetrations detected at the interfaces. This contact force is proportional to the penetration depth and the larger the penetrations, the larger the contact force applied to the interacting bodies. The contact boundary conditions can be interpreted as a spring placed between the two bodies as illustrated in Figure 2.1. Typically, the higher the spring's stiffness (contact stiffness) and the larger the penetration depth, the larger the contact force applied to the interacting surfaces. It should be noted that numerical instability of the contact algorithm may be induced if the contact stiffness is too large. The penalty method utilizes a slave-master approach to handle contact between interacting surfaces: one as the slave and the other as the master surface. Either surface can be assigned as the slave surface when using a symmetric penalty method. However, it is recommended that the slave surface be the one with finer meshes. Currently, there are three implementations of the penalty method in LS-DYNA: the standard penalty formulation, the soft constraint penalty formulation, and the segment-based penalty formulation.

The standard penalty formulation is the most commonly used method for calculating contact forces between interacting bodies. In this method, each slave node is checked against the master surface for penetrations. If a penetration is detected, a contact

force is calculated and applied to the slave nodes as well as the nodes on the master surface to move the two interacting bodies away from each other and thus eliminate the penetration. The contact force f is obtained by

$$f = -lk \tag{2.1}$$

where k is the contact stiffness of the master segment and *l* is the penetration depth of the slave node. The contact stiffness, k_{solid}, of a solid element is calculated by

$$k_{solid} = \frac{fKA^2}{V} \tag{2.2}$$

where *K* is the bulk modulus, *V* is the volume and *A* is the face area of the solid element. Similarly, the contact stiffness of a shell element is given by

$$k_{shell} = \frac{f_s KA}{max(shell\ diagonal)} \tag{2.3}$$

Examination of Eqs. (2.2) and (2.3) indicates that the magnitude of the contact spring stiffness is contingent upon the size of the contact segment as well as the element's material properties. Therefore, it is not recommended to use the standard penalty approach for contacts involving bodies with dissimilar materials. Furthermore, the low bulk modulus of very soft materials can significantly lower the contact stiffness and eventually lead to excessive penetrations. For contact scenarios involving very soft materials, it is possible to manually scale the contact stiffness to ensure contact stability. An alternative to scaling the contact stiffness for soft materials is to use the soft constraint penalty formulation.

In the soft constraint penalty formulation, an additional contact stiffness is introduced to eliminate the inherent penetrations observed in contacts involving dissimilar or very soft materials with the standard penalty approach. The additional contact stiffness,

$k_{stability}$, which is referred to as the stability contact stiffness, is calculated based on the nodal masses that come into contact and the global time step size and is given by

$$k_{stability} = 0.5 \cdot \text{SOFSCL} \cdot m^* \cdot \left(\frac{1}{\Delta t}\right)^2 \tag{2.4}$$

where SOFSCL is a soft scale factor for the Soft Constraint Penalty Formulation, m^* is the total mass of both the slave and master nodes (i.e., the sum of nodal masses), and Δt is the timestep. The stability contact stiffness is compared with the stiffness obtained using the standard penalty formulation and the larger one is used as the interface contact stiffness.

Another type of penalty formulation is the segment-based penalty formulation, which is similar to the soft constraint penalty formulation. In the segment-based penalty formulation, an additional contact stiffness is also incorporated. The additional contact stiffness, $k_{segment}$, is independent of the material properties and is calculated based on the segment masses rather than the nodal masses.

$$k_{segment} = 0.5 \cdot \text{SLSFAC} \cdot \begin{Bmatrix} \text{SFS} \\ \text{or} \\ \text{SFM} \end{Bmatrix} \left(\frac{m_1 m_2}{m_1 + m_2}\right)\left(\frac{1}{\Delta t}\right)^2 \tag{2.5}$$

where SLSFAC is the sliding interface scale factor, SFS is the slave segment stiffness scale factor, SFM is the master segment stiffness scale factor, m_1 and m_2 are the masses of the slave and master segment, respectively, and Δt is the timestep. Evaluation of Eq. (2.5) results in

$$k_{segment1} = 0.5 \cdot \text{SLSFAC} \cdot \{\text{SFS}\} \left(\frac{m_1 m_2}{m_1 + m_2}\right)\left(\frac{1}{\Delta t}\right)^2 \tag{2.6}$$

$$k_{segment2} = 0.5 \cdot \text{SLSFAC} \cdot \{\text{SFM}\} \left(\frac{m_1 m_2}{m_1 + m_2}\right)\left(\frac{1}{\Delta t}\right)^2 \tag{2.7}$$

The stiffness obtained from Eqs. (2.6) and (2.7) is compared with the stiffness obtained using the standard penalty formulation and the maximum stiffness is taken as the interface contact stiffness.

2.2 Contact Algorithms in LS-DYNA

Several contact algorithms have been implemented into LS-DYNA since its first release in 1976. The contact algorithms differ primarily by the search algorithm utilized to detect penetrations and the method of enforcing contact boundary conditions. Earlier contact algorithms, referred to as the non-automatic contact types, utilized search algorithms that checked for contact from only one side of a shell element. Automatic contact types were subsequently introduced as an enhancement of the older contact algorithms. The search algorithm employed by automatic contact types are more robust and can detect potential penetration from either side of a shell element. Automatic contact types use bucket sorting technique in its search algorithm. The bucket sorting approach involves identifying possible master contact segments for each slave node. If penetration is detected, any of the preciously discussed penalty-based methods can be used to enforce the user-specified contact boundary conditions. Penalty-based contact algorithm can be categorized into one-way contacts, two-way contacts, and single surface contacts. Further details of the various catepenalty-based contact and its implementation in LSDYNA are discussed next.

One-way contact is commonly used for analysis involving a rigid master surface and deformable slave surface. As the name aptly suggests, the one-way contact only checks for penetration of the slave nodes through master segments. The one-way contact allows the transfer of compression and tangential loads between the slave nodes and the master

segments. In addition, it is well-suited for analysis involving beam-to-surface or shell-edge-to-surface scenarios. One-way contact has both automatic and non-automatic forms. Commonly used non-automatic one-way contact include nodes_to_surface and one_way_surface_to_surface, with the automatic equivalents given as automatic_nodes_to_surface and automatic_one_way_surface_to_surface, respectively. The choice of master or slave surface can significantly affect the performance of one-way contacts. An example is illustrated in Figure 2.2. In the first case, the impactor is assigned the slave surface while the impacted surface is assigned the master surface. The master and slave surface assignments were reversed in the second case. As seen in Figure 2.2 (b), one-way contact failed to detect the penetration of the master node through the slave surface because it only searches for penetration of a slave node through a master surface.

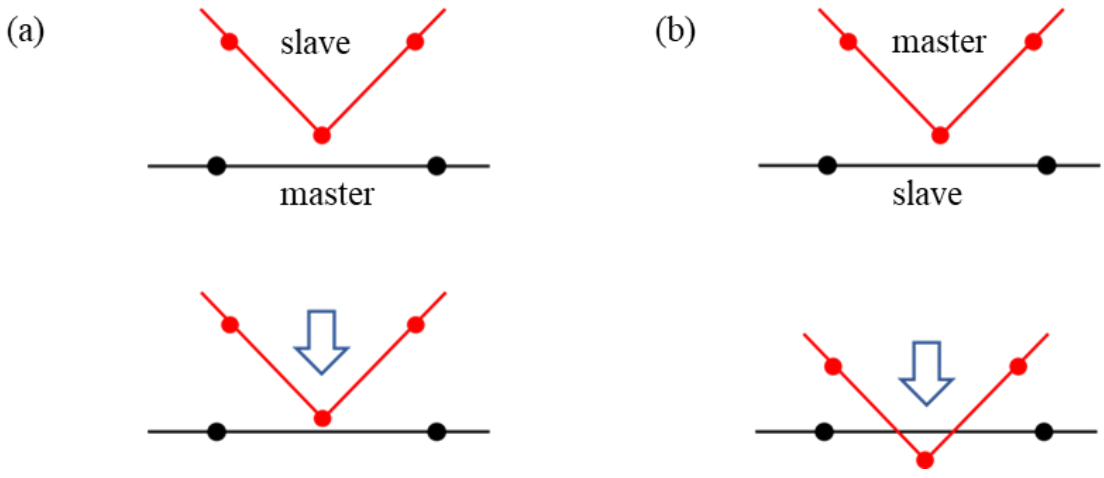

Figure 2.2: Illustration of one-way contact treatment. (a) Penetration is detected and eliminated. (b) Contact failed to detect penetration because the slave node has not penetrated through the master segment.

A similar contact type to one-way contact treatment, is the two-way contact types. The two-way contact works by checking for penetration of each slave node through the

master segment and for penetration of each master node through the slave segment. This means that the results will be the same regardless of what surface is defined as the master or slave segment making it more robust than the one-way contact treatment. Because penetration is checked twice, it is computationally more expensive than the one-way contact treatment. Similar to the one-way contact types, the two-way contact types have both automatic and non-automatic forms. Commonly used two-way contacts include automatic_surface_to_surface and surface_to_surface. A limitation of the two-way contact types is that it is unable to detect self-contact. For self-contact situations, the single surface contact types are recommended.

The most widely used penalty-based contact types are the single surface contact types. Single surface implies that contact is defined wholly by the slave side. Single surface contacts check for contacts between the parts defined in a contact set as well as self-contact of each part. There is no

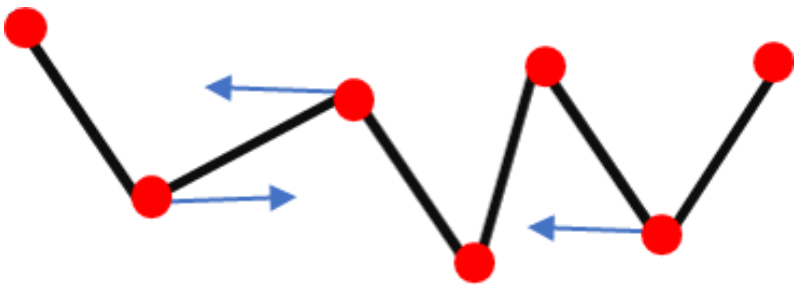

Figure 2.3: Self-contact is checked in single-surface contact types.

need to define a master surface in single surface contacts. An illustration of single surface contact is shown in Figure 2.3. Single surface contacts are computationally more expensive than the other penalty-based contacts. Commonly used single surface contacts include automatic_general and automatic_single_surface. Automatic_general is ideal for analysis involving shell edge-to-edge, beam-to-beam, and beam-to-shell edge contact. In addition,

automatic_general has an option that checks for internal shell edges contact. This is known as automatic_general_interior. A less computationally expensive form of automatic_general is automatic_single_surface. Automatic_single_surface is the most commonly used single surface contact for crash simulations.

CHAPTER 3: FINITE ELEMENT MODELING

This chapter presents the detailed work on the FE models of a two-bar metal bridge and simulation setup for the full-scale crash tests. The process involved creating the geometry of the bridge rail, meshing the components, defining sectional and material properties, assigning contacts, prescribing initial velocity to the vehicles, and imposing necessary boundary conditions.

Figure 3.1 shows an actual NC two-bar metal bridge rail along with the corresponding FE model. Full-scale crash tests of the bridge rail were conducted under MASH TL-3 conditions. i.e.,

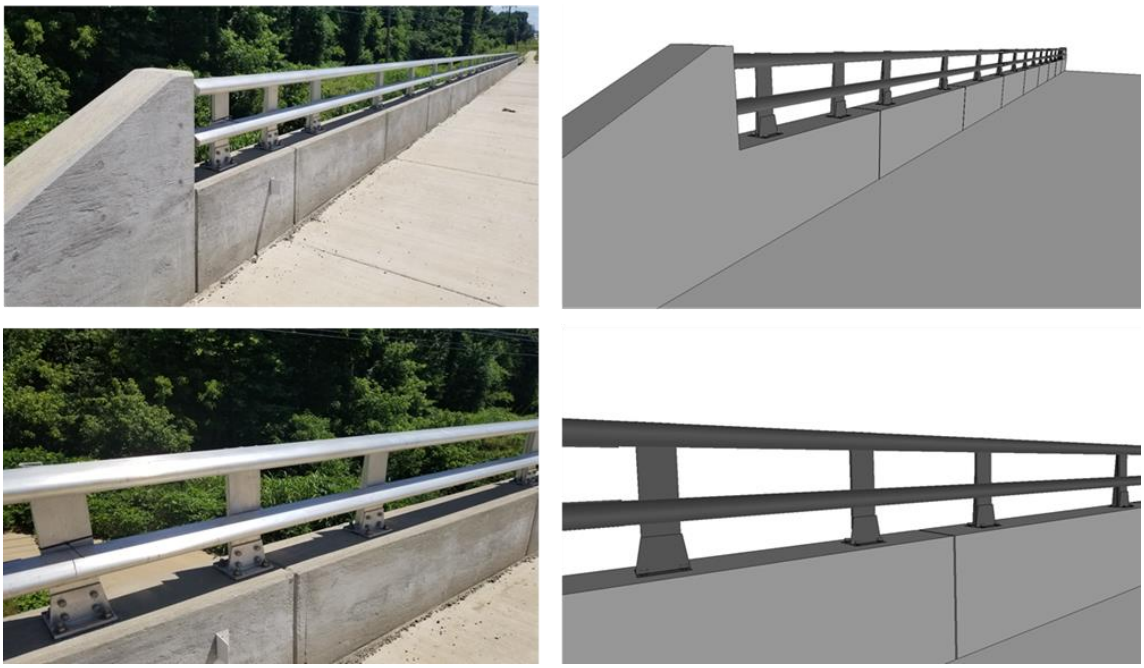

Figure 3.1: A two-bar bridge rail (a) and the finite model (b).

under vehicular impacts by a small passenger car (1100C) and a pickup truck (2270P) at an impact speed of 62 mph (100 km/hr) and an impact angle of 25°. The FE element models of a 2007 Chevy Silverado quad-cab pick-up truck and a 2010 Toyota Yaris passenger

sedan were used as the test vehicles in the simulations. Additionally, the FE model of a 2014 Chevy Silverado pick-up truck, which was a newer version of the FE model than the 2007 Chevy Silverado, was also used to conduct the same simulation so as to compare the results obtained using both the old and new Chevy Silverado models. Table 3.1 gives the details of the MASH TL-3 test conditions.

Table 3.1: MASH TL-3 Test conditions for Longitudinal Barriers.

Test No.	Test Vehicle	Vehicle Designation (MASH)	Test Vehicle Mass lb. (kg)	Impact Conditions	
				Speed	Angle
1	Yaris	1100C	2420 (1,100)	62 mph (100km/hr)	25°
2	Silverado (2007)	2270P	5000 (2,270)		
3*	Silverado (2014)	2270P	5000 (2,270)		

*Additional simulation (MASH TL-3 only requires two test vehicles: a passenger car and a pickup truck)

3.1 FE Models of Test Vehicles

The test vehicles, shown in Figures 3.2 and 3.3, were originally developed at NCAC and validated against frontal and side impact tests. In addition, the vehicle models have been used in several full-scale crash testing of roadside safety devices.

The FE models of both the 2007 and 2014 Silverado had a total mass of 5,000 lbs. (2,270 kg) and met the requirements for a 2270P test vehicle specified by MASH. The 2007 Silverado model had 721 parts (components) discretized into 963,482 elements with an average mesh size of 0.3 in. (8 mm). The 2014 Silverado model had 1501 parts discretized into 2,960,781 elements with an average mesh size of 0.24 in. (6 mm). The FE model of the 2010 Toyota Yaris met the MASH requirements for a 1100C test vehicle; it

had a total mass of 2,420 lbs. (1,100 kg) and was composed of 919 parts that were discretized into 1,519,587 elements with an average mesh size of 0.31 in. (8 mm).

All the three vehicle models included fully functional suspension and steering subsystems. An accelerometer, which had a constitutive model of rigid material, was positioned at the center of gravity (CG) of the test vehicle to record the acceleration histories during the simulation. Further details of the geometry, material properties and model development of the vehicle models are documented in the NCAC reports on model validation (NCAC web2).

Figure 3.2: The FE model of a 2010 Toyota Yaris passenger sedan.

Figure 3.3: The FE models of a 2007 (left) and a 2014 (right) Chevy Silverado quad-cab pick-up truck.

3.2 FE Model of a Two-bar Bridge Rail

The FE model of the two-bar bridge rail consisted of aluminum posts, elliptical rails, and base plates on top of a concrete parapet. The length of the bridge rail was 90 ft

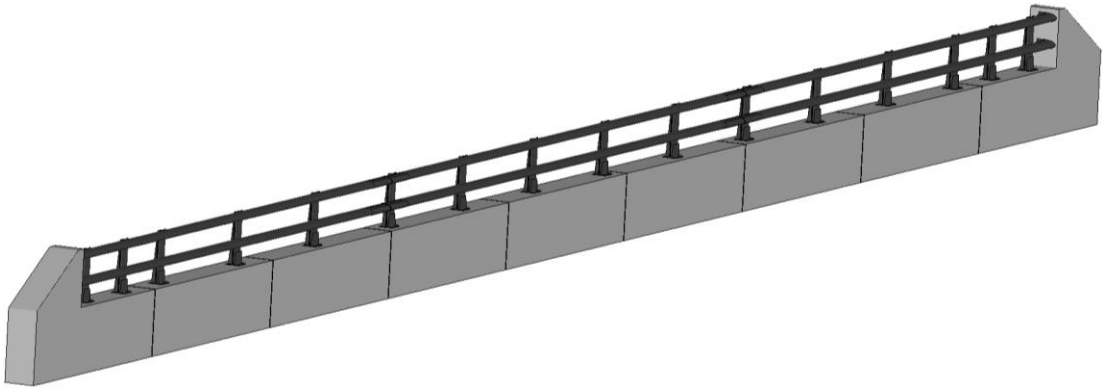

Figure 3.4: The FE model of a two-bar bridge rail.

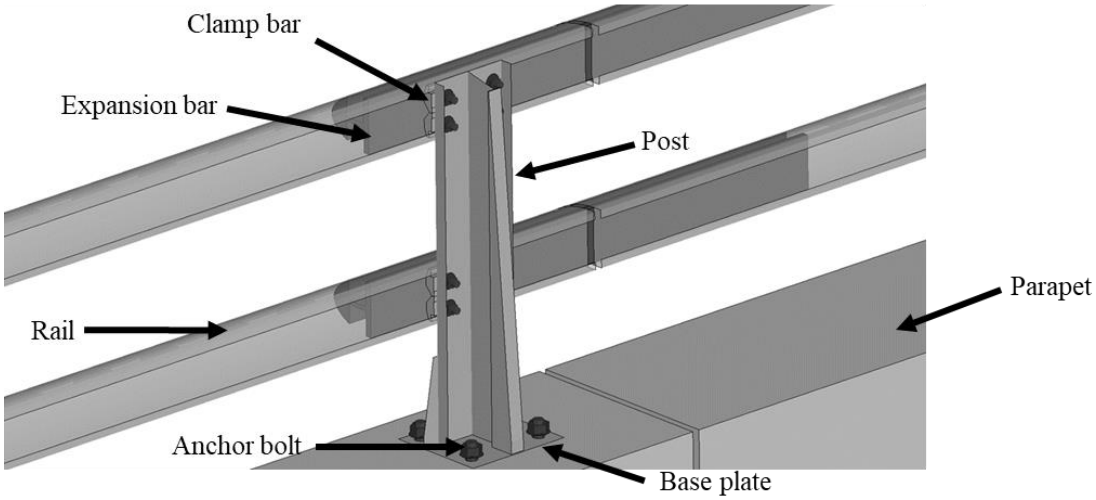

Figure 3.5: Closeup view of some of the components of the bridge rail model.

(27432 mm) and the height was 52 in (1,422 mm) above grade. The bridge rail model was discretized into 4,856,352 elements with an average mesh size of 0.5 in. (12.7 mm). Figure 3.4 shows the FE model of the two-bar bridge rail. Figure 3.5 shows a closeup view of a

bridge rail post and the connected components including the clamp bar, expansion bar, aluminum post, elliptical rail, base plate anchor bolts, and parapets.

The concrete parapet, as shown in Figure 3.6, was discretized into 3,863,416 solid elements with reduced integration and Flanagan-Belytschko hourglass control (i.e., using the exact volume integration formulation). An elastoplastic constitutive model with damage and rate effects was utilized to model the concrete parapet. The implementation of this concrete's material model in LS-DYNA was given by *MAT_CSCM_CONCRETE, whose input parameters were obtained from a study by Murray et.al (2004) titled "Evaluation of LS-DYNA Concrete Material Model

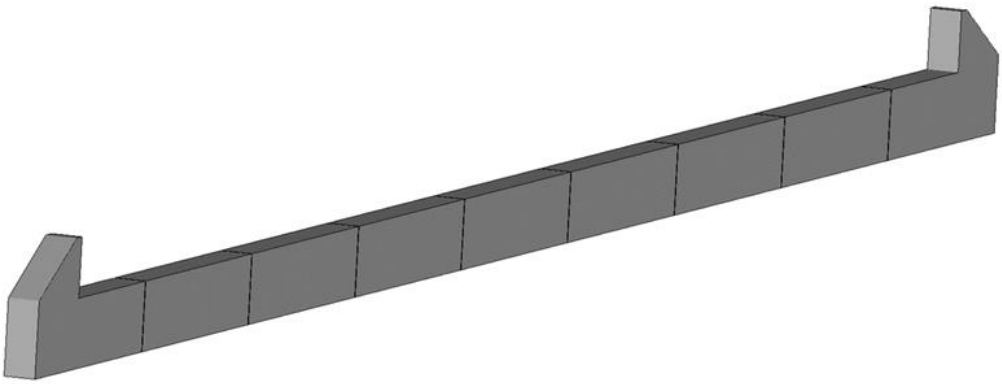

Figure 3.6: The FE model of a concrete parapet.

159". The parapet consisted of horizontal and vertical steel-bar reinforcement that was explicitly modelled throughout the entire length of the parapet, as shown in Figure 3.7. The node-sharing technique was used to model the steel reinforcement in the parapet, i.e., the

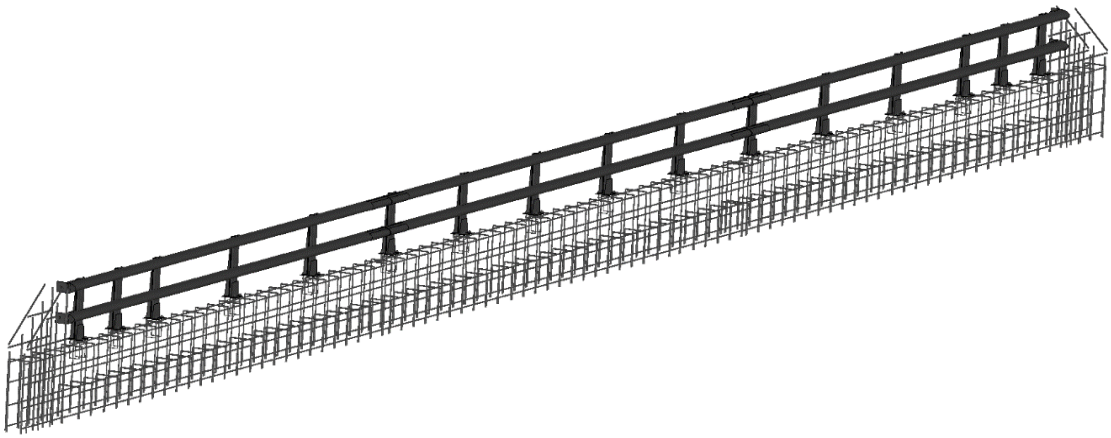

Figure 3.7: Steel reinforcement in the concrete parapet.

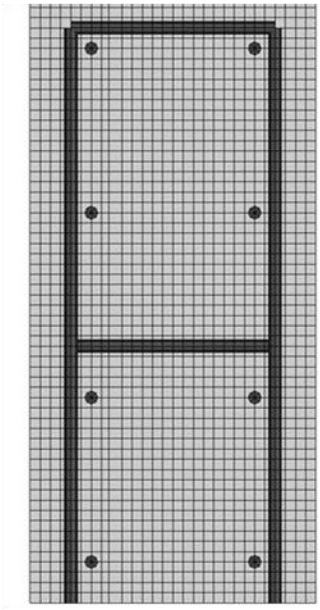

Figure 3.8: Cross-sectional view of the concrete parapet with horizontal and vertical steel reinforcement.

steel bars were modelled using beam elements whose nodes were aligned with nodes of the solid elements for the parapet. Figure 3.8 shows the cross-sectional view of the concrete parapet with the embedded horizontal and vertical steel bars sharing nodes with the nodes of the solid elements used to model the concrete parapet. The steel bars were modelled using Hughes-Liu beam elements with an average mesh size of ½ -inch (12.7 mm) and a

piecewise linear plasticity material model. The boundary conditions for the bridge rail were applied by fixing the bottom nodes of the parapet and the vertical reinforcement.

Figure 3.9 (a) shows the detailed post assembly including the aluminum post, clamp bar base plate, and anchor bolts assembly. The aluminum post was meshed using a combination of shell and solid elements. As shown in Figure 3.9(b), null shells were used on the interface between the shell elements for the front face of post and the solid elements for the rear section of the post.

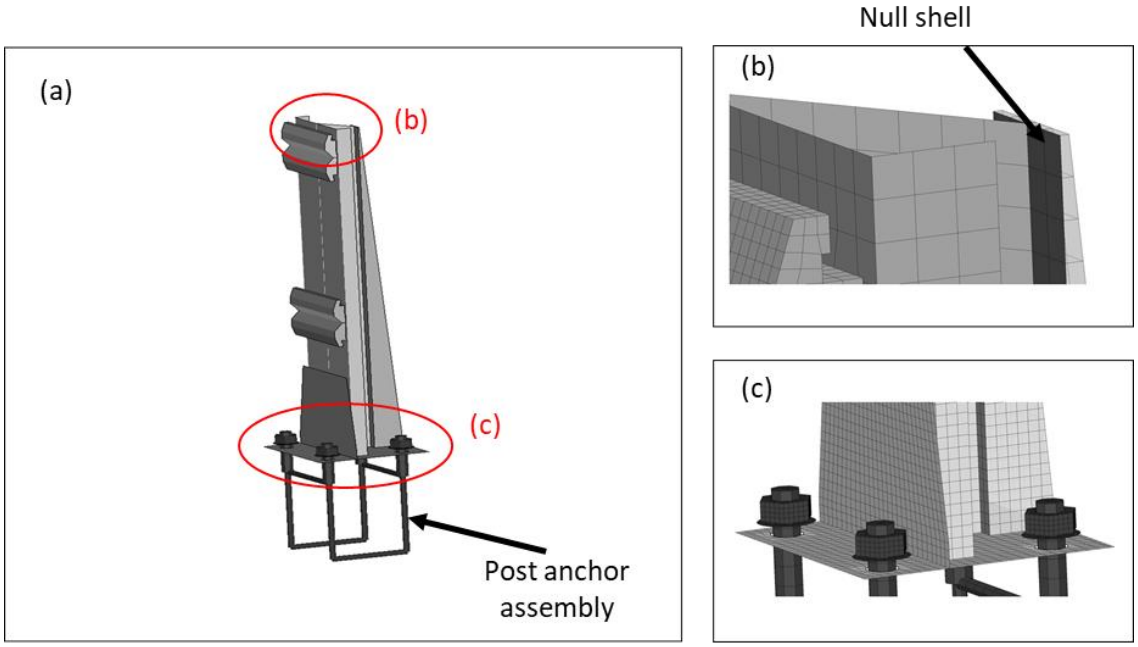

Figure 3.9: Post anchor assembly.

The base plate was meshed using fully integrated shell elements and the clamp bars were discretized using solid elements. Beam elements were used to model the anchor bolts as well as the anchor assembly. Pre-tensioning of the bolts was achieved using discrete spring. Similar to the reinforcement, the nodes of the anchor bolts and steel reinforcement were merged with the nodes of the parapet. The elliptical rails, which were mounted to the

clamp bars, were meshed using fully integrated shell elements. The extension bars, which were used to connect elliptical rails, were modelled using solid elements. A piecewise linear plasticity constitutive model was defined for the elliptical rails, aluminum posts, clamp bars, expansion bars, and steel bolts.

3.3 Simulation setup

The bridge rail was combined with each of the three test vehicles to perform the crash simulations. The impact locations were determined in accordance with the specifications recommended by MASH. The impact location of the Yaris was located at 54.6-in (1,386 mm) from the mid-point of the aluminum post closest to the expansion bar in the rails. Similarly, the impact location of the Silverado was determined at 61.9-in (1573 mm) from the mid-point of the aluminum post closest to the expansion bar in the rails. The impact location for the Silverado is shown in Figure 3.10.

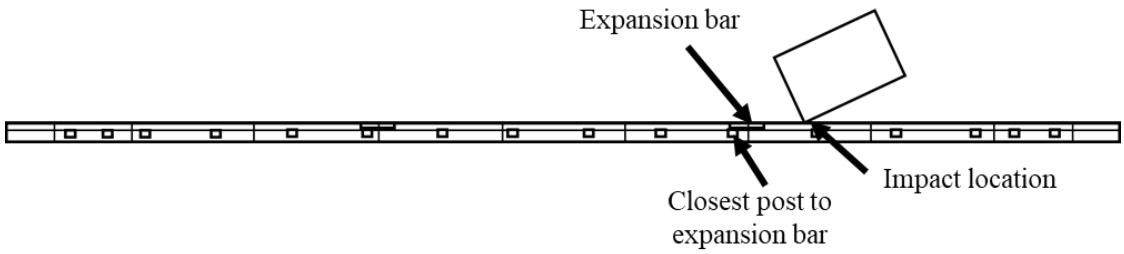

Figure 3.10: Impact location of the Silverado model.

Figures 3.11 to 3.13 show the top and front views of the simulation setup for the three vehicle models. It can be seen from Figures 3.11 to 3.13 that the impact location of

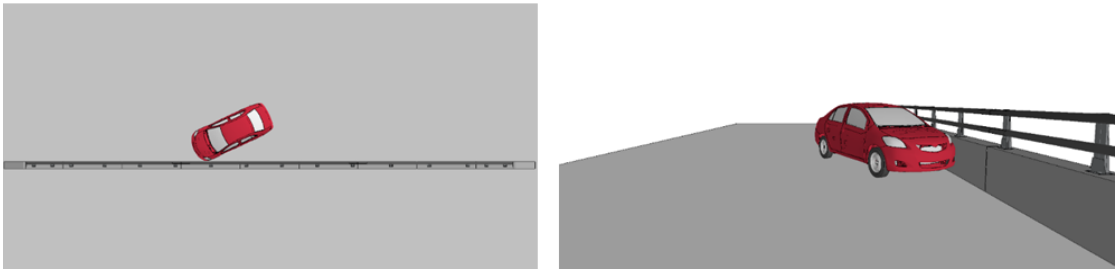

Figure 3.11: Simulation setup for the 2010 Toyota Yaris impacting the bridge rail.

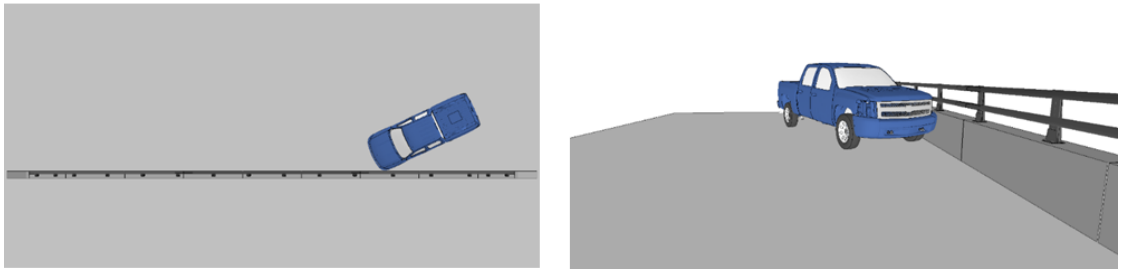

Figure 3.12: Simulation setup for the 2007 Chevy Silverado impacting the bridge rail.

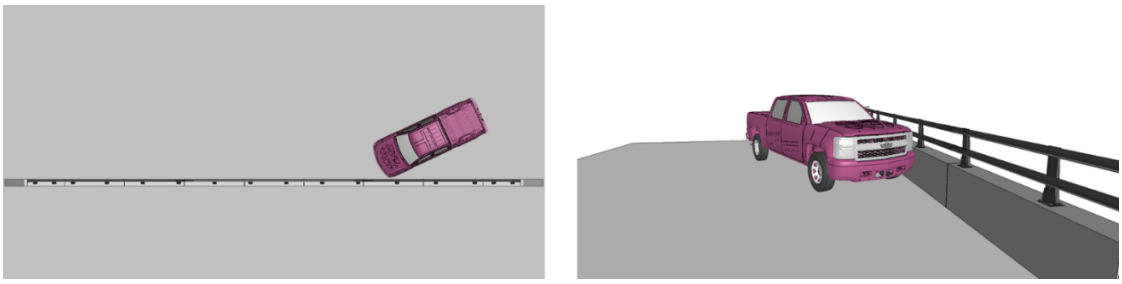

Figure 3.13: Simulation setup for the 2014 Chevy Silverado impacting the bridge rail.

the Yaris model is further downstream compared to the impact location of the Silverado models. This was done to ensure that the simulation setup was the same as those of the actual full-scale crash tests. The pre-processor and FE solver used for this research were Hypermesh and LS-DYNA, respectively. The simulation results are discussed in the next chapter.

CHAPTER 4: PERFORMANCE EVALUATION OF TWO-BAR BRIDGE RAIL

In this chapter, the simulation results are presented for two full-scale crash tests of the two-bar bridge rail under MASH TL-3 conditions, i.e., impacted by a 1100C and a 2270P vehicle, respectively, at an impact speed of 62 mph (100 km/hr.) and at a 25° angle. In the simulations of this study, a 2010 Toyota Yaris was used as the 1100C vehicle, and a 2007 Chevy Silverado and a 2014 Chevy Silverado were used as the 2270P vehicle. The impact locations for the 1100C and 2270P vehicles were located at 54.6-in (1386 mm) and 61.9-in (1573 mm), respectively, from the mid-points of the aluminum posts closest to the splices in the rails (see Figures 3.10 to 3.13 for details). It should be noted that the MASH TL-3 criterion only required one 1100C and one 2270P vehicle. The 2014 Chevy Silverado (2270P) was added to this study because it was obtained after the research had already begun using the 2007 Chevy Silverado model. In the actual crash tests on the bridge rail, the 1100C and 2270P vehicles were a 2010 Hyundai Accent and a 2015 Chevy Silverado. Although the vehicles used in simulating the crash tests were different from the ones used in the actual crash tests, they still fall under the same classification according to MASH and thus, were comparable.

In order to evaluate the impact performance of the bridge rail, three factors were examined: structural adequacy, occupant risk, and post-impact trajectory of the vehicle. The structural adequacy was assessed using MASH evaluation criterion *A*, which requires the barrier to contain and redirect the vehicles. In addition, the vehicle should not override, underride or penetrate the barrier. The occupant risk was assessed using MASH evaluation criteria *D*, *F* and *H*. MASH evaluation criterion *D* specifies that debris from the barrier as a result of the crash should not intrude into the occupant compartment or pose hazard to

pedestrians. MASH evaluation criterion *F* requires the vehicle to remain upright throughout the entire impact and not exceed a maximum roll and pitch angles of 75°. MASH evaluation criterion *H* specifies two occupant risk parameters, Occupant Impact Velocity (OIV) and the Occupant Ridedown Acceleration (ORA), that can be used to assess the risk of occupant injuries. The OIV and ORA are calculated in both longitudinal and lateral directions, and according to MASH, the preferred limits for OIV and ORA are 9.1 *m/s* and 15.0 *g*, respectively. The acceptable values for OIV and ORA are 12.20 *m/s* and 20.49 *g*, respectively. The ORA in the longitudinal or lateral direction is obtained by taking the maximum values of longitudinal or lateral accelerations averaged over 10 *ms* after the vehicle impacts the barrier. The longitudinal and lateral accelerations were obtained from the vehicle's CG point.

The possibility of the impacting vehicle getting involved in a secondary crash with other vehicles was evaluated by examining the vehicle's post-impact trajectory. Excessive pocketing or snagging of the vehicle into the barrier could lead to unsafe post-impact trajectory such as spin-outs or high vehicular exit angle. Ideally, the barrier should contain and smoothly redirect the vehicle without any penetration of the vehicle behind the barrier. In this study, the MASH exit box criterion was used to assess the post-impact response of the vehicles. It should be noted that satisfying the exit box criterion is not required for the Two-bar bridge rail but was computed for information purpose only. The exit box is defined by a rectangle whose length is parallel to the traffic side of the barrier and starts at the final point of contact of the wheel track with the initial traffic face of the barrier. A graphical illustration of the exit box and exit angle is shown in Figure 4.1. The exit box dimensions of the Toyota Yaris, the 2007 Chevy Silverado and the 2014 Chevy Silverado

are given in Table 4.1. The exit box criterion is satisfied if the vehicle's wheel tracks are within the exit box before the vehicle exits the right side of the box. In addition to the exit box criterion, the longitudinal and lateral accelerations, velocities and displacements were also obtained from the accelerometer placed at the vehicle's CG point. The accelerometer data were subsequently filtered using an SAE Class 60 filter.

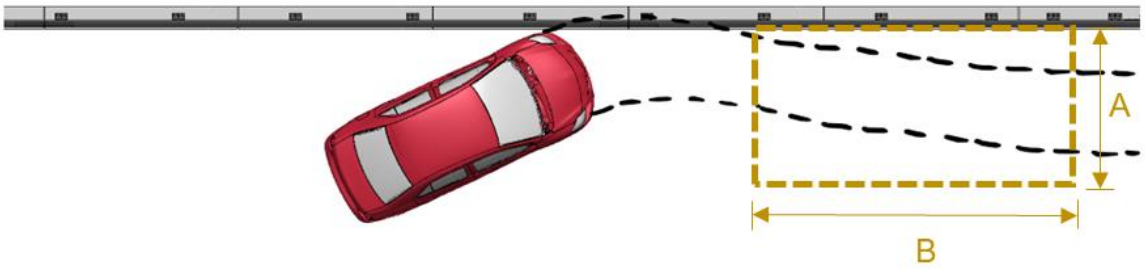

Figure 4.1: Exit box illustration for test vehicles.

Table 4.1: Exit box dimensions for test vehicles.

Vehicle	**A**	**B**
2010 Toyota Yaris	15.1 ft (4.6 m)	32.8 ft (10.0 m)
2007 Chevy Silverado	16.9 ft (5.15 m)	32.8 ft (10.0 m)
2014 Chevy Silverado	16.9 ft (5.15 m)	32.8 ft (10.0 m)

4.1 Impact by the 2010 Toyota Yaris

In this section, the two-bar bridge rail was evaluated under impact of a 2010 Toyota Yaris at a speed of 62 mph (100 km/hr.) and a of 25° angle. The simulation results were compared to test data of a 2010 Hyundai Accent impacting the two-bar bridge rail under

the same conditions. Figure 4.2 shows the exit box along with the two-bar bridge rail in its original state and the vehicle wheel track highlighted in black. As seen in Figure 4.2, the exit box criterion was satisfied. The exit angle of the 2010 Toyota Yaris was calculated to be 6.09°.

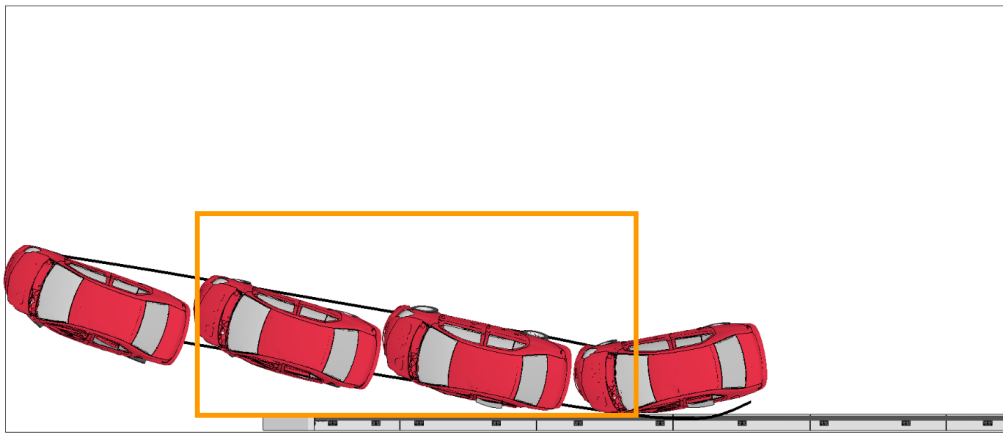

Figure 4.2: A 2010 Toyota Yaris impacting the Two-bar bridge rail.

Figure 4.3 shows a comparison of the longitudinal (*x*-axis) and lateral (*y*-axis) accelerations of the simulation results (in red color) and the actual test data (in blue color). It was observed that the acceleration profiles of the Toyota Yaris in the simulation results were similar to the actual test data. Figure 4.4 shows the longitudinal (*x*-axis) and lateral (*y*-axis) velocities of simulation results compared to those of the actual test data. Figure 4.5 shows the comparison of the longitudinal (*x*-axis) and lateral (*y*-axis) displacements of simulation results and actual test data. It was obseverd that the velocity and displacement profiles of the Toyota Yaris were similar to the actual test data.

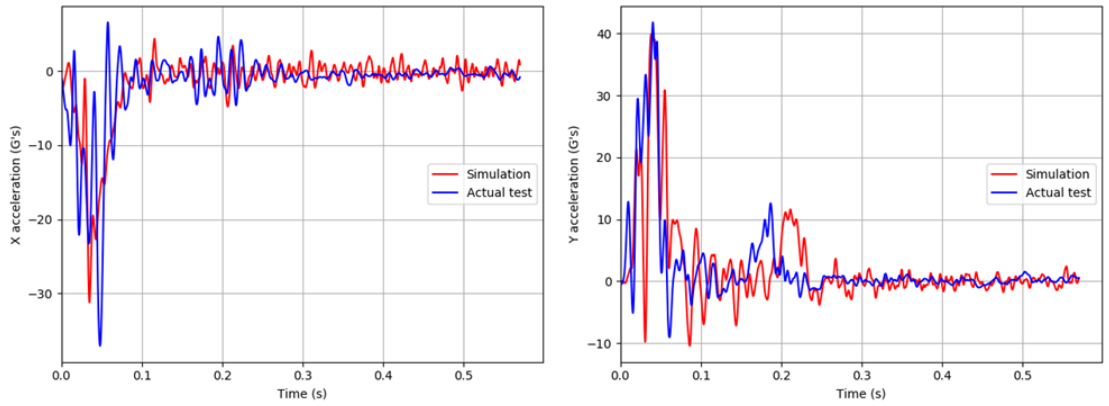

Figure 4.3: Comparison of *x* and *y* acceleration-time histories of Toyota Yaris impact and actual test result.

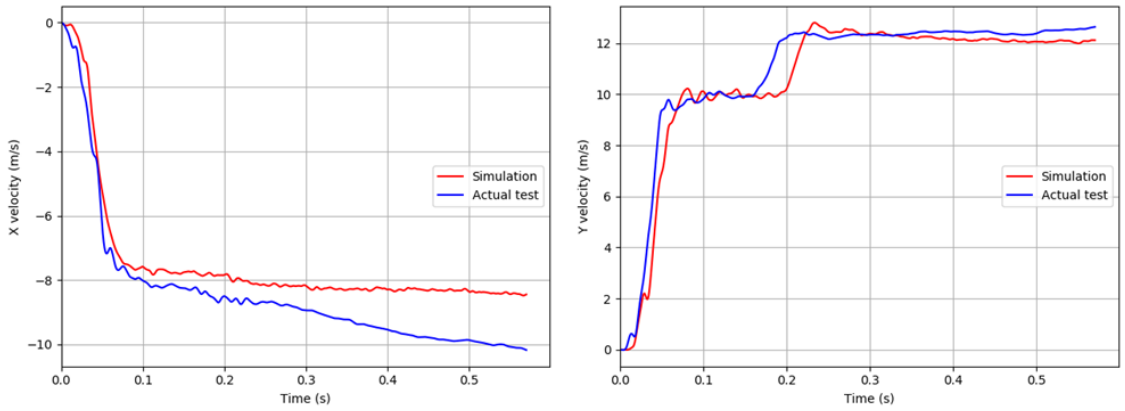

Figure 4.4: Comparison of *x* and *y* velocity-time histories of Toyota Yaris impact and actual test result.

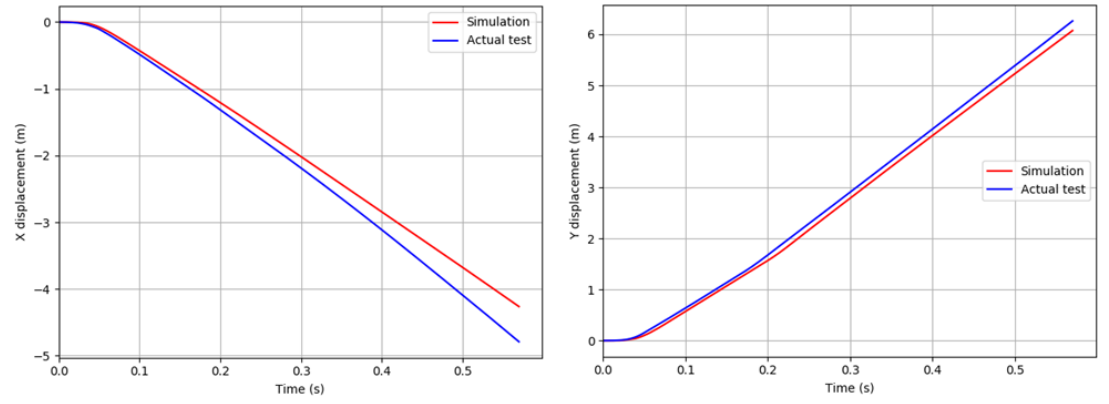

Figure 4.5: Comparison of *x* and *y* displacement-time histories of Toyota Yaris impact and actual test result.

The yaw, pitch and roll angles of the Toyota Yaris were compared with the actual crash test data of the 2010 Hyundai Accent, as shown in Figures 4.6 to 4.8. The yaw angles of the Toyota Yaris throughout the impact had similar trend as the test data (Figure 4.6). The pitch angles of the Toyota Yaris had similar trend to those of the test vehicle except for those within the first 0.1 seconds (Figure 4.7). The roll angles of the Toyota Yaris also had a similar trend to those of the test vehicle for the most part of the impact except for the time when the Yaris started impacting the barrier (Figure 4.8). The discrepancies of pitch and roll angles between simulation results and test data could be caused by the structural differences of the two vehicles, even though both were MASH compliant. The difference in pitch angles between the 2010 Hyundai Accent and the 2010 Toyota Yaris could be caused by some of the structural differences such as the differences in the stiffness of the suspensions and the types of steering system. For example, the 2010 Hyundai Accent had an electric power steering, while the 2010 Toyota Yaris used a hydraulic power steering. Nevertheless, the overall trends of yaw, pitch and roll angles of the vehicle in the simulation were similar to those of the test vehicle. The pitch and roll angles of the Toyota Yaris were less than 75°, which satisfied the requirement of MASH criterion *F*.

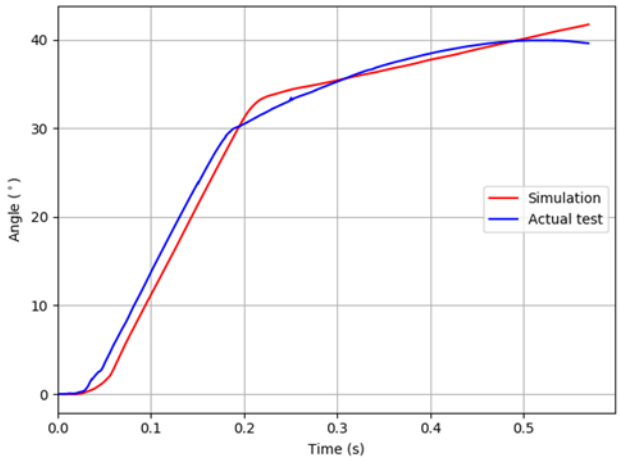

Figure 4.6: Comparison of yaw angles of Toyota Yaris impact and actual test result.

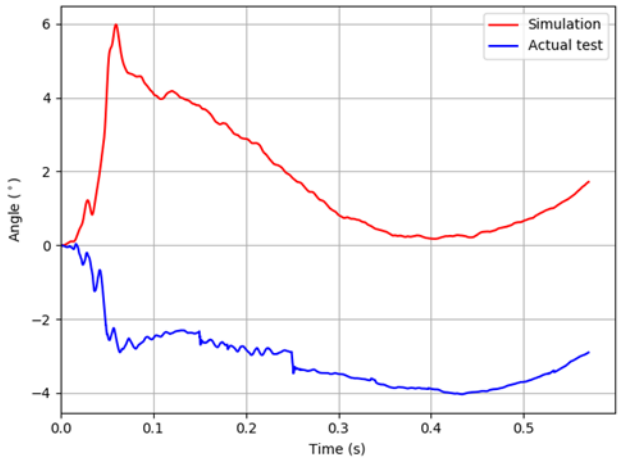

Figure 4.7: Comparison of pitch angles of Toyota Yaris impact and actual test result.

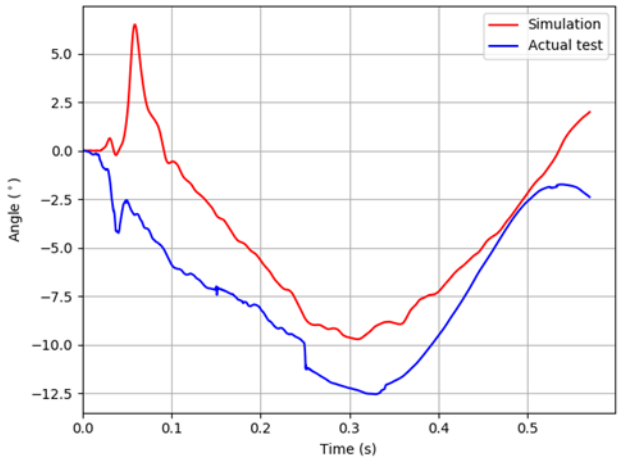

Figure 4.8: Comparison of roll angles of Toyota Yaris impact and actual test result.

The occupant risk factors, i.e., OIVs and ORAs, were computed from the acceleration data from simulation results and were compared to test data. Table 4.2 gives a summary of the occupant risk factors for the simulation and actual test.

Table 4.2: Summary of occupant risk factors computed for Toyota Yaris.

Occupant Risk Factors		**Simulation result**	**Actual Test**	**Difference**		**MASH Limits**
				Absolute	**%**	
OIV (*m/s*)	Longitudinal (*x*-axis)	-7.33	-7.45	0.12	1.611	12.20
	Lateral (*y*-axis)	-9.84	-9.38	0.46	4.90	
ORA (*g*)	Longitudinal (*x*-axis)	-2.31	-3.65	1.340	36.7	20.5
	Lateral (*y*-axis)	-10.25	-10.20	0.05	0.49	

The comparison in Table 4.2 showed that the simulation results generally agreed well with test data. The largest discrepancy occurred on the ORA in longitudinal direction, which had a 36.7% relative error. It should be noted that there was no specified limit in MASH for the maximum allowable difference between simulation results and test data for the occupant risk factors. In the NCHRP Report W179, it was suggested that the difference between FEA results and test values for each occupant risk factor be less than 20 percent unless the magnitude was relatively small. Since the ORA values in the longitudinal direction, both from simulation results and test data, were way below the MASH limit, the

ORAs and OIVs from simulation results were considered to be acceptable based on the limit values given in Report W179. In addition, all the OIVs and ORAs were below the MASH limit values; therefore, the MASH criterion *H* was satisfied.

The vehicular response and the deformation of the barrier were also examined. The Toyota Yaris had minimal contact with the lower and top rail. The damages to the vehicle were mostly on the impact side. Parts on the impact side with the most deformations were the fender, headlight, hood, and doors. The vehicle was safety contained and redirected, thus satisfying MASH evaluation criterion *A*. Figure 4.9 shows an instance of the Toyota Yaris impacting the barrier and Figure 4.10 shows a post-impact snapshot of the barrier. It was observed that the "erosion" of the concrete parapet was minimal. There was a small deformation of the base plates under the post at the initial impact location. The examination of debris and vehicle deformation from the simulation results indicated that MASH evaluation criteria *D* was satisfied.

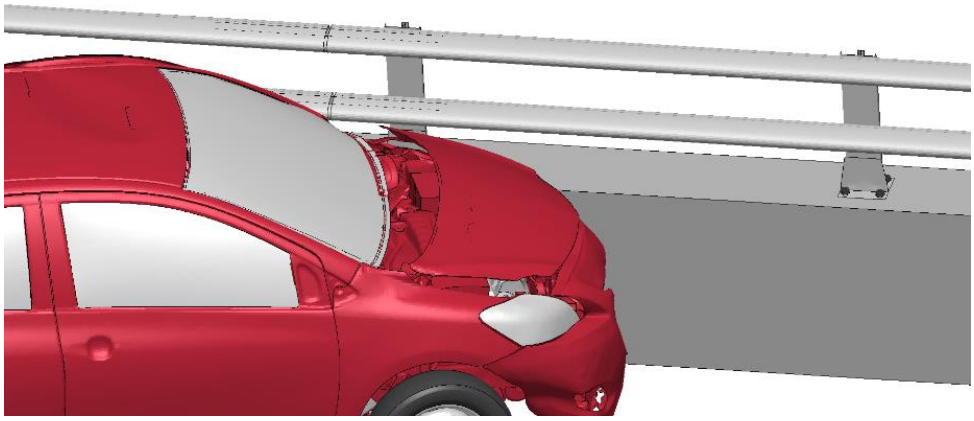

Figure 4.9: Toyota Yaris impacting the Two-bar bridge rail.

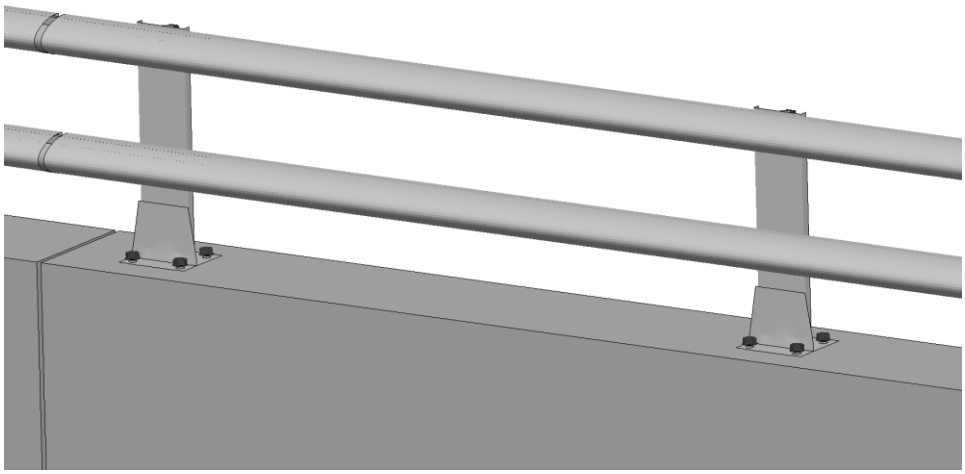

Figure 4.10: Snapshot of Two-bar bridge rail after impact.

Table 4.3 gives a summary of the simulation results for the Toyota Yaris with respect to the MASH evaluation criteria. As shown in the table, the two-bar bridge rail performed well under the impact of the 2010 Toyota Yaris.

Table 4.3: Summary of simulation results for Toyota Yaris.

Mash Evaluation Criteria	**Result**
A	Passed
D	Passed
E	Passed
F	Passed
H	Passed
Exit box	Passed

4.2 Impact by the 2007 Chevy Silverado

In this section, the two-bar bridge rail was evaluated under impact of a 2007 Chevy Silverado at a speed of 62 mph (100 km/hr.) and a of 25° angle. The simulation results were compared to test data of a 2015 Chevy Silverado impacting the two-bar bridge rail under the same conditions. Figure 4.11 shows the exit box along with the two-bar bridge rail in its original state and the vehicle wheel track highlighted in black. As seen in Figure 4.11, the exit box criterion was satisfied. The exit angle of the 2007 Chevy Silverado was calculated to be 5.93°.

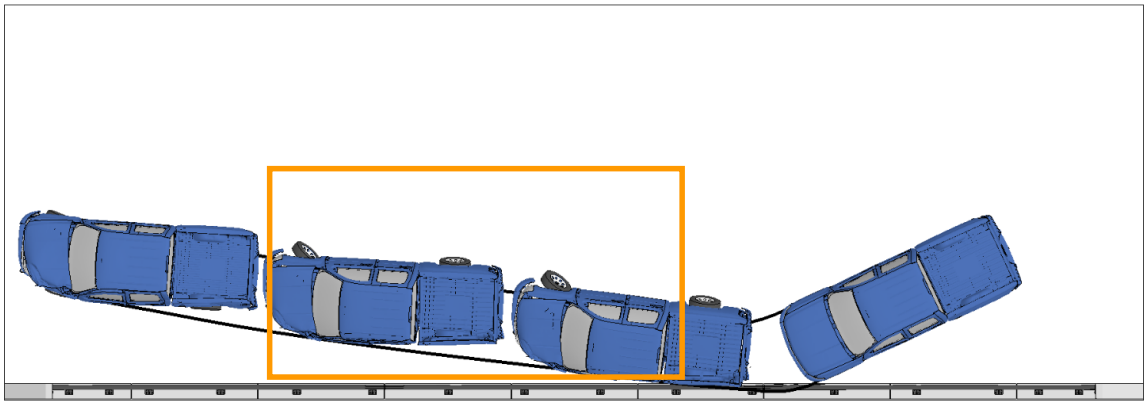

Figure 4.11: A 2007 Chevy Silverado impacting the Two-bar bridge rail.

Figure 4.12 shows a comparison of the longitudinal (*x*-axis) and lateral (*y*-axis) accelerations of the simulation results (in red color) and the actual test data (in blue color). It was observed that the acceleration profiles of the 2007 Chevy Silverado in the simulation results were similar to the actual test data. Figure 4.13 shows the longitudinal (*x*-axis) and lateral (*y*-axis) velocities of simulation results compared to those of the actual test data. It was observed that the velocity and displacement profiles of the 2007 Chevy Silverado is similar to the actual test result.

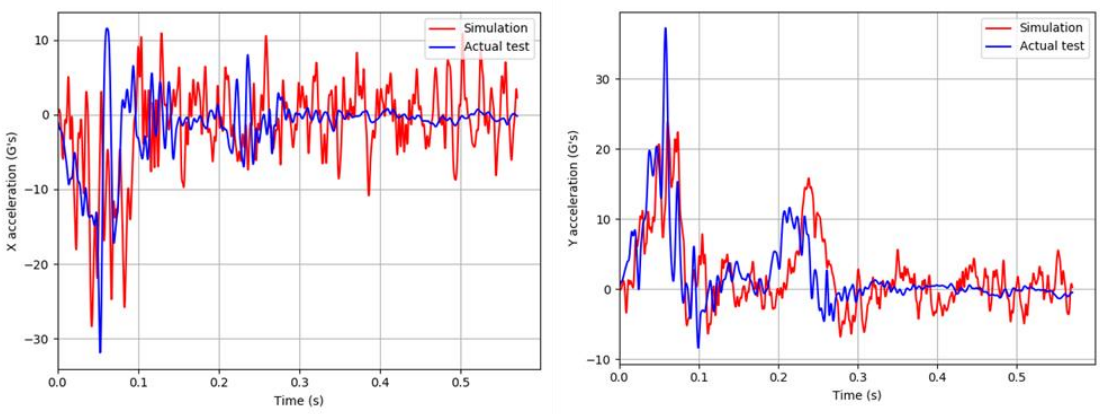

Figure 4.12: Comparison of *x* and *y* acceleration-time histories of 2007 Chevy Silverado impacting the Two-bar bridge rail.

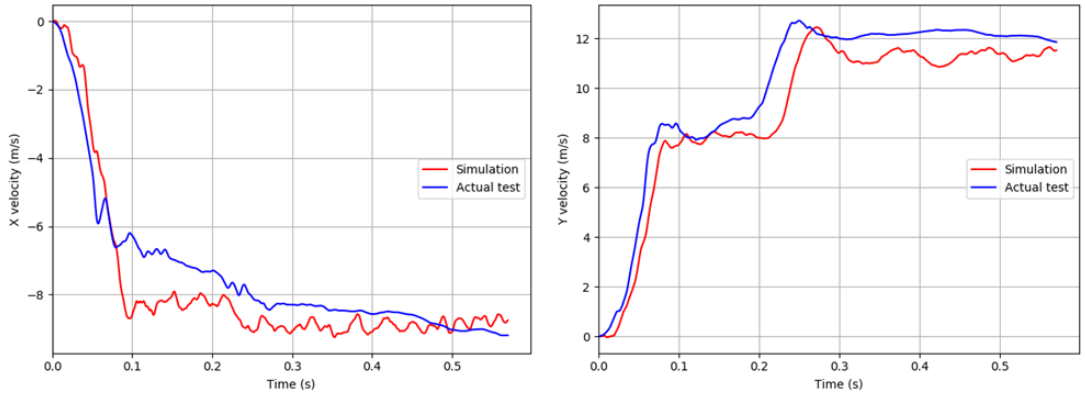

Figure 4.13: Comparison of x and y velocity-time histories of 2007 Chevy Silverado impacting the Two-bar bridge rail.

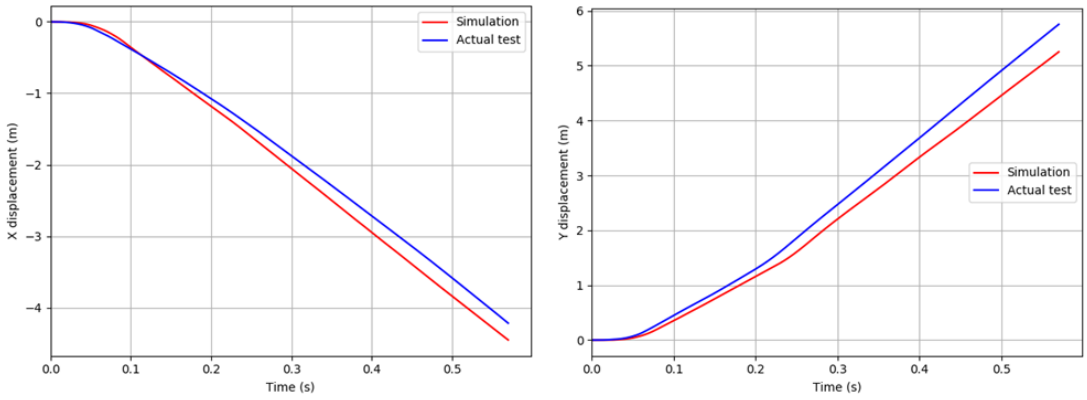

Figure 4.14: : Comparison of x and y displacement-time histories of 2007 Chevy Silverado impacting the Two-bar bridge rail.

The yaw, pitch and roll angles of the 2007 Chevy Silverado were compared with the actual crash test data of the 2015 Chevy Silverado, as shown in Figures 4.15 to 4.17. The yaw angles of the Chevy Silverado throughout the impact had similar trend as the test data (Figure 4.15). The pitch angles of the Chevy Silverado had similar trend to those of the test vehicle except for those within the first 0.1 seconds (Figure 4.16). The roll angles of the Chevy Silverado also had a similar trend to those of the test vehicle for the most part of the impact (Figure 4.17). The discrepancies of roll angles between simulation results and test data could be caused by the structural differences of the two vehicles, even though both were MASH compliant. Nevertheless, the overall trends of yaw, pitch and roll angles of the vehicle in the simulation were similar to those of the test vehicle. The pitch and roll angles of the Chevy Silverado were less than 75°, which satisfied the requirement of MASH criterion *F*.

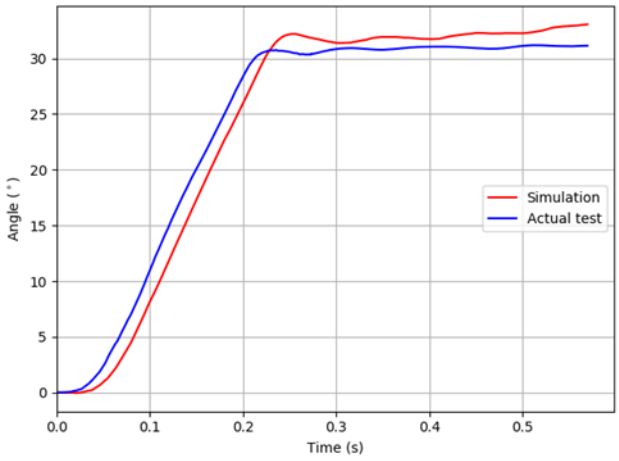

Figure 4.15: Comparison of yaw angle of 2007 Chevy Silverado impact and actual test result.

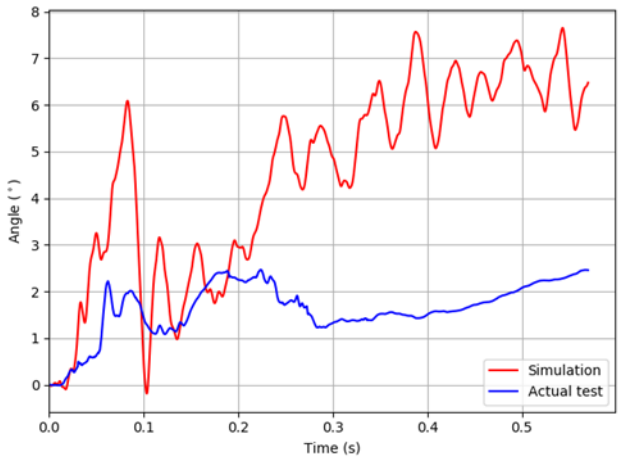

Figure 4.16: Comparison of pitch angle of 2007 Chevy Silverado impact and actual test result.

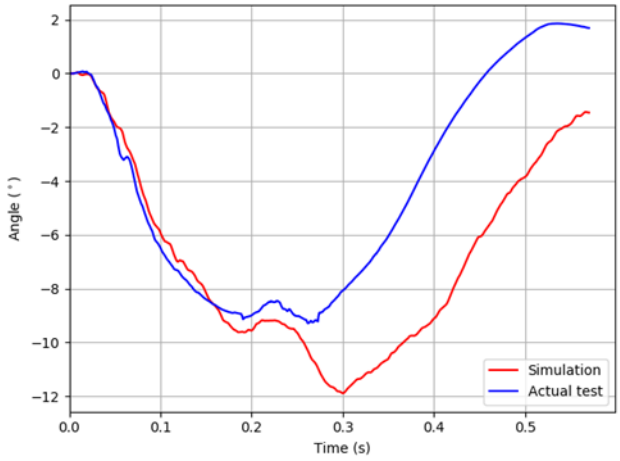

Figure 4.17: Comparison of roll angle of 2007 Chevy Silverado impact and actual test result.

The occupant risk factors, i.e., OIVs and ORAs, were computed from the acceleration data from simulation results and were compared to test data. Table 4.4 gives a summary of the occupant risk factors for the simulation and actual test.

Table 4.4: Summary of occupant risk factors computed for 2007 Chevy Silverado.

Occupant Risk Factors		**Simulation result**	**Actual Test**	**Difference**		**MASH Limits**
				Absolute	**%**	
OIV (*m/s*)	Longitudinal (*x*-axis)	-8.21	-6.55	1.66	25.3	12.20
	Lateral (*y*-axis)	-7.72	-8.50	0.78	9.17	
ORA (*g*)	Longitudinal (*x*-axis)	-5.87	-5.09	0.78	15.32	20.5
	Lateral (*y*-axis)	-13.26	-10.78	2.48	23.0	

The comparison in Table 4.4 showed that the simulation results generally agreed well with test data. The largest discrepancy occurred on the ORA in longitudinal direction, which had a 25.3% relative error. It should be noted that there was no specified limit in MASH for the maximum allowable difference between simulation results and test data for the occupant risk factors. In the NCHRP Report W179, it was suggested that the difference between FEA results and test values for each occupant risk factor be less than 20 percent unless the magnitude was relatively small. Since the ORA values in the longitudinal direction, both from simulation results and test data, were below the MASH limit, the ORAs and OIVs from simulation results were considered to be acceptable based on the

limit values given in Report W179. In addition, all the OIVs and ORAs were below the MASH limit values; therefore, the MASH criterion *H* was satisfied.

The vehicular response and the deformation of the barrier were also examined. The 2007 Chevy Silverado had contact with both the lower and top rail, and the concrete parapet. The damages to the vehicle were mostly on the impact side. Parts on the impact side with the most deformations were the bumper, fender, headlight, hood and doors. Figure 4.18 shows an instance of the Chevy Silverado impacting the barrier and Figure 4.19 shows a post-impact snapshot of the barrier. It was observed that the "erosion" of the concrete parapet was moderate. The "erosion" of the concrete parapet mainly occurred at the impact location. The deformation of the rails and posts were minimal. The examination of debris and the vehicle deformation in the simulation results indicated that MASH evaluation criteria *D* was satisfied.

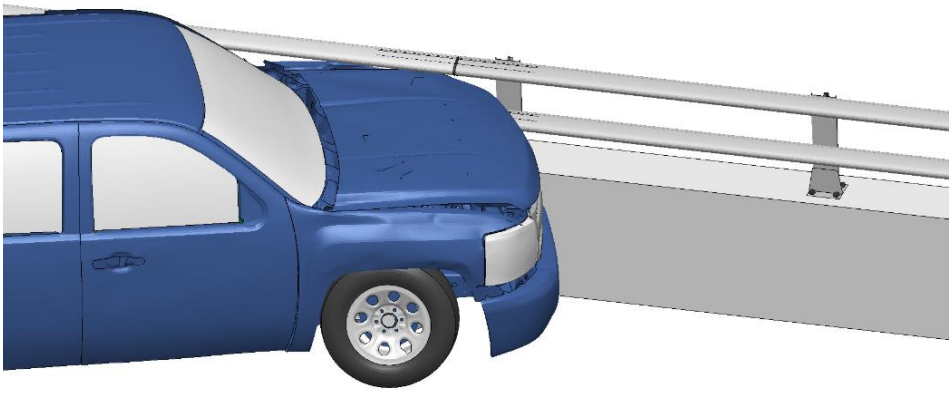

Figure 4.18: 2007 Chevy Silverado impacting the Two-bar bridge rail.

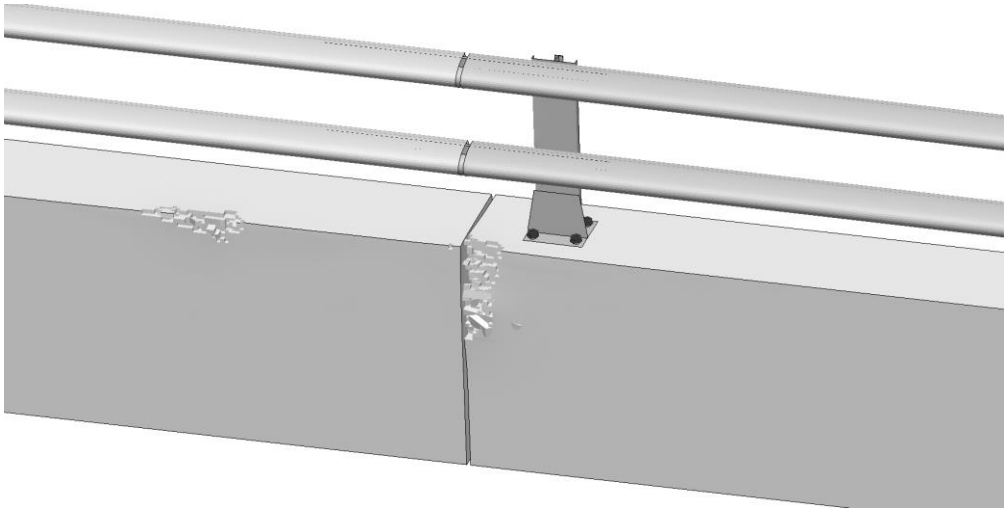

Figure 4.19: Snapshot of Two-bar bridge rail after impact.

Table 4.5 gives a summary of the simulation results for the 2007 Chevy Silverado with respect to the MASH evaluation criteria. As shown in the table the two-bar bridge rail performed well in for the 2007 Chevy Silverado impacts.

Table 4.5: Summary of simulation results for 2007 Chevy Silverado.

Mash Evaluation Criteria	**Result**
A	Passed
D	Passed
E	Passed
F	Passed
H	Passed
Exit box	Passed

4.3 Impact by the 2014 Chevy Silverado

In this section, the two-bar bridge rail was evaluated under impact of a 2014 Chevy Silverado at a speed of 62 mph (100 km/hr.) and a of 25° angle. The simulation results were compared to test data of a 2015 Chevy Silverado impacting the two-bar bridge rail under the same conditions. Figure 4.20 shows the exit box along with the two-bar bridge rail in its original state

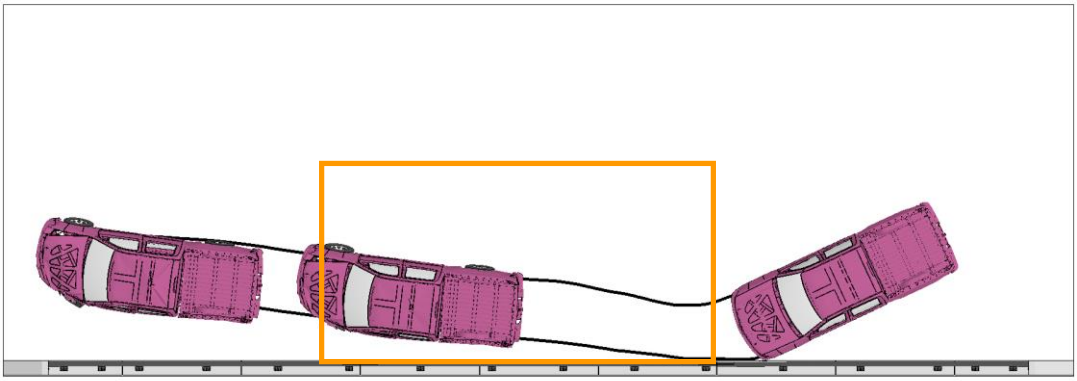

Figure 4.20: A 2014 Chevy Silverado impacting the Two-bar bridge rail.

and the vehicle wheel track highlighted in black. As seen in Figure 4.20, the exit box criterion was satisfied. The exit angle of the 2014 Chevy Silverado was calculated to be 6.82°.

Figure 4.21 shows a comparison of the longitudinal (*x*-axis) and lateral (*y*-axis) accelerations of the simulation results (in red color) and the actual test data (in blue color). It was observed that the acceleration profiles of the 2014 Chevy Silverado in the simulation results were similar to the actual test data. Figure 4.21 shows the longitudinal (*x*-axis) and lateral (*y*-axis) velocities of simulation results compared to those of the actual test data. It

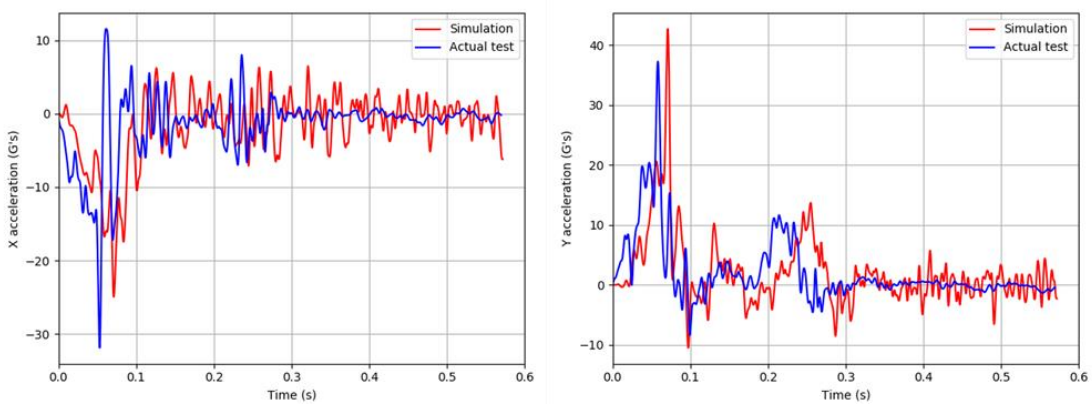

Figure 4.21: Comparison of x and y acceleration-time histories 2014 Chevy Silverado impacting the Two-bar bridge rail.

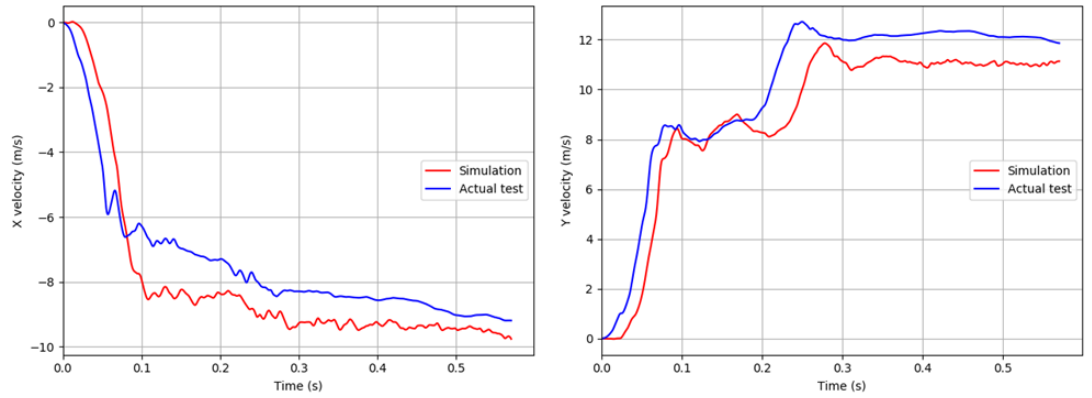

Figure 4.22: Comparison of x and y velocity-time histories of 2014 Chevy Silverado impacting the Two-bar bridge rail.

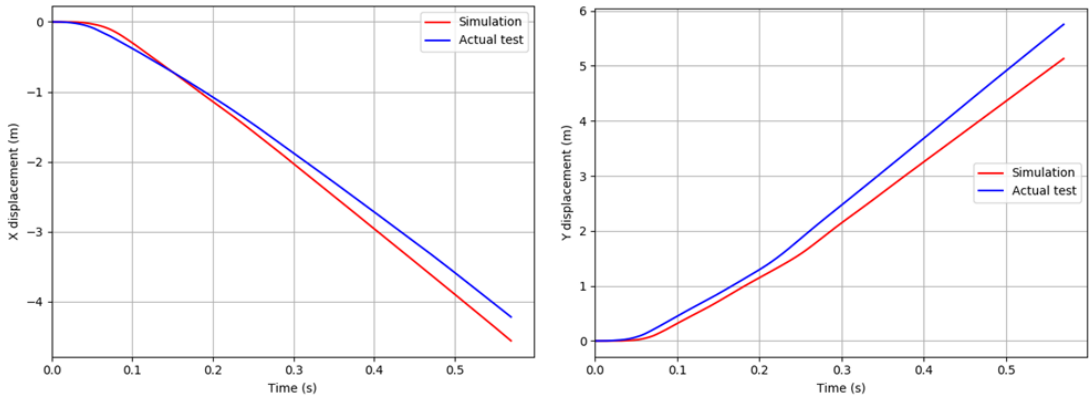

Figure 4.23: Comparison of x and y displacement-time histories of 2014 Chevy Silverado impacting the Two-bar bridge rail.

was observed that the velocity and displacement profiles of the 2014 Chevy Silverado is similar to the actual test result.

The yaw, pitch and roll angles of the 2014 Chevy Silverado were compared with the actual crash test data of the 2015 Chevy Silverado, as shown in Figures 4.24 to 4.26. The yaw angles of the Chevy Silverado throughout the impact had similar trend as the test data (Figure 4.24). The pitch angles of the Chevy Silverado had similar trend to those of the test vehicle except for those after 0.3 seconds (Figure 4.25). The roll angles of the Chevy Silverado also had a similar trend to those of the test vehicle for the most part of the impact (Figure 4.26). The overall trends of yaw, pitch and roll angles of the vehicle in the simulation were similar to those of the test vehicle. The

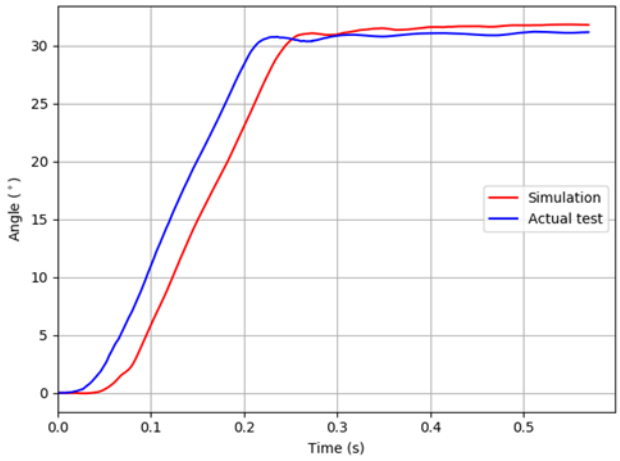

Figure 4.24: Comparison of yaw angle of 2014 Chevy Silverado impact and actual test result.

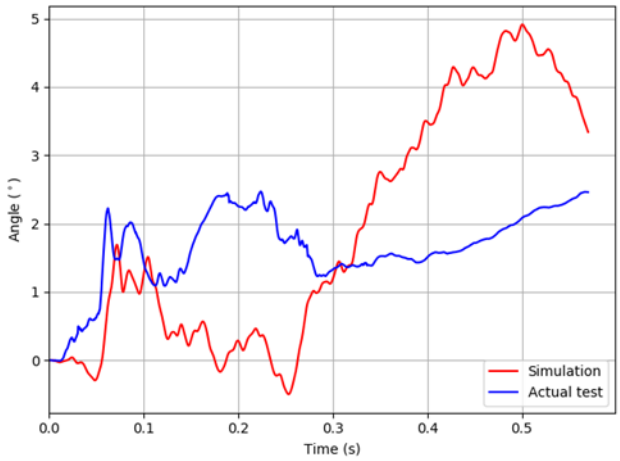

Figure 4.25: Comparison of pitch angle of 2014 Chevy Silverado impact and actual test result.

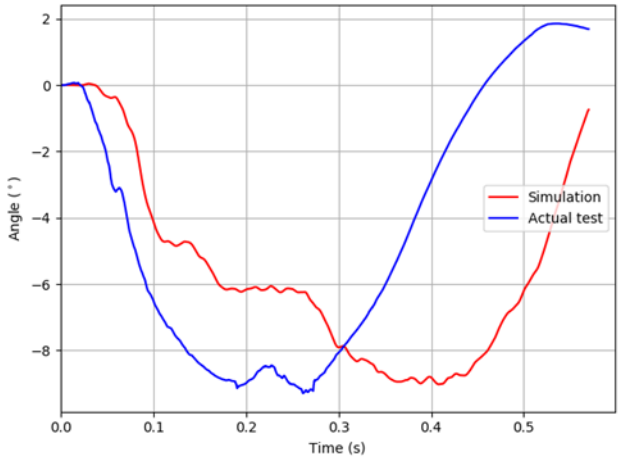

Figure 4.26: Comparison of roll angle of 2014 Chevy Silverado impact and actual test result.

pitch and roll angles of the Chevy Silverado were less than 75°, which satisfied the requirement of MASH criterion *F*.

The occupant risk factors, i.e., OIVs and ORAs, were computed from the acceleration data from simulation results and were compared to test data. Table 4.6 gives a summary of the occupant risk factors for the simulation and actual test.

Table 4.6: Summary of occupant risk factors computed for 2014 Chevy Silverado.

Occupant Risk Factors		**Simulation result**	**Actual Test**	**Difference**		**MASH Limits**
				Absolute	**%**	
OIV (*m/s*)	Longitudinal (*x*-axis)	-7.88	-6.55	1.330	20.3	12.20
	Lateral (*y*-axis)	-8.18	-8.50	0.32	3.76	
ORA (*g*)	Longitudinal (*x*-axis)	-6.85	-5.09	1.760	34.5	20.5
	Lateral (*y*-axis)	-10.97	-10.78	0.19	1.762	

The comparison in Table 4.6 showed that the simulation results generally agreed well with test data. The largest discrepancy occurred on the ORA in longitudinal direction, which had a 34.5% relative error. Since the ORA values in the longitudinal direction, both from simulation results and test data, were below the MASH limit, the ORAs and OIVs from simulation results were considered to be acceptable based on the limit values given in Report W179. In addition, all the OIVs and ORAs were below the MASH limit values; therefore, the MASH criterion *H* was satisfied.

The vehicular response and the deformation of the barrier were also examined. The 2014 Chevy Silverado had contact with both the lower and top rail, and the concrete parapet. The damages to the vehicle were mostly on the impact side. Parts on the impact side with the most deformations were the suspension, bumper, fender, headlight, hood and

doors. The vehicle was safety contained and redirected, thus satisfying MASH evaluation criterion *A*. Figure 4.27 shows an instance of the 2014 Chevy Silverado impacting the barrier and Figure 4.28 shows a post-impact snapshot of the barrier. It was observed that the "erosion" of the concrete parapet was moderate. There was a small deformation of the rails and the posts at the initial impact location. The examination of debris and the vehicle deformation in the simulation result indicates that MASH evaluation criteria *D* was satisfied.

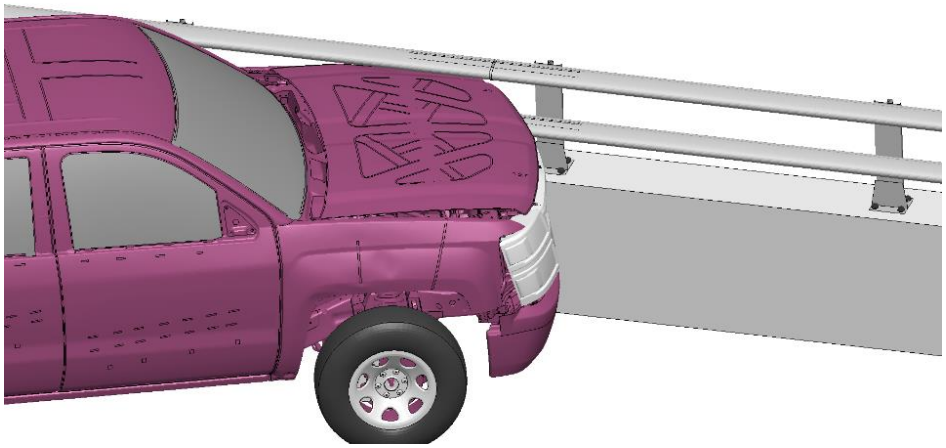

Figure 4.27: 2014 Chevy Silverado impacting the Two-bar bridge rail.

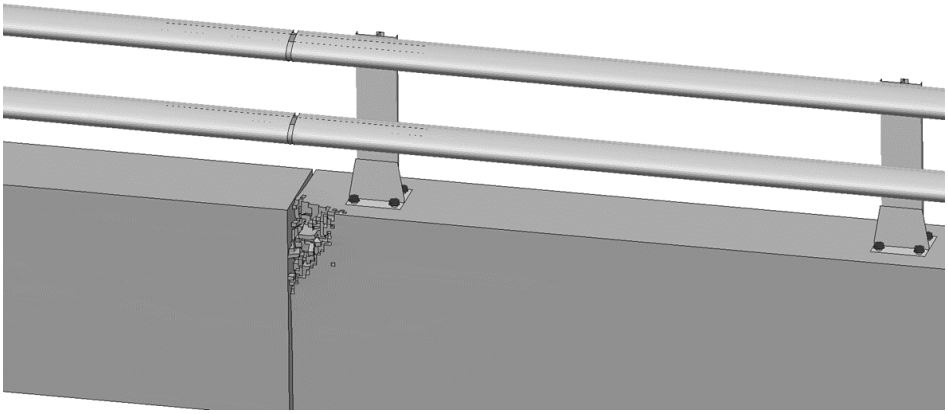

Figure 4.28: Snapshot of Two-bar bridge rail after impact.

Table 4.7 gives a summary of the simulation results for the 2014 Chevy Silverado with respect to the MASH evaluation criteria. As shown in the table, the two-bar bridge rail performed well under the impact of the 2014 Chevy Silverado.

Table 4.7 Summary of simulation results for 2014 Chevy Silverado.

Mash Evaluation Criteria	**Result**
A	Passed
D	Passed
E	Passed
F	Passed
H	Passed
Exit box	Passed

CHAPTER 5: SUMMARY AND CONCLUSIONS

The objective of this study was to use FE simulations to evaluate the performance of a two-bar bridge rail under MASH test level 3 (TL-3) conditions, i.e., under impacts of a 1100C and a 2270P vehicle, respectively, at an impact speed of 62 mph (100 km/hr.) and at a 25° angle. In the simulations of this study, a 2010 Toyota Yaris was used as the 1100C vehicle, and a 2007 Chevy Silverado and a 2014 Chevy Silverado were used as the 2270P vehicle. A detailed FE model of an NCDOT two-bar bridge rail was fully developed in this research to evaluate the impact performance under MASH TL-3 conditions. The 90 ft two-bar bridge rail consisted of aluminum posts, elliptical rails, and base plates on top of a concrete parapet. The steel reinforcement in the concrete parapet was explicitly modeled by merging the nodes of the reinforcement with the nodes of the solid elements used in modeling the concrete parapet. The simulation results were also compared to test data. In the actual crash tests on the bridge rail, the 1100C and 2270P vehicles were a 2010 Hyundai Accent and a 2015 Chevy Silverado. Although the vehicles used in simulating the crash tests were different from the ones used in the actual crash tests, they still fall under the same classification according to MASH and thus, were comparable.

In order to evaluate the impact performance of the bridge rail, three factors were examined: structural adequacy, occupant risk, and post-impact trajectory of the vehicle. The MASH evaluation criteria *A*, *D*, *F*, and *H* were used to access the three performance factors. MASH evaluation criterion *A* requires the barrier to contain and redirect the vehicles. MASH evaluation criterion *D* specifies that debris from the barrier as a result of the crash should not intrude into the occupant compartment or pose hazard to pedestrians. MASH evaluation criterion *F* requires the vehicle to remain upright throughout the entire

impact and not exceed a maximum roll and pitch angles of 75°. MASH evaluation criterion *H* specifies that the Occupant Impact Velocity (OIV) and the Occupant Ridedown Acceleration (ORA) not exceed 12.20 *m/s* and 20.49 *g*, respectively. The MASH exit box criterion, exit angles, and the time histories of the vehicles' velocities, accelerations, and displacements were also examined.

The simulation results showed that the acceleration, velocity and displacement profiles of the 2010 Toyota Yaris were similar to the actual test data. The vehicle was safety contained and redirected, thus satisfying MASH evaluation criterion *A*. The examination of debris and vehicle deformation from the simulation results indicated that MASH evaluation criteria *D* was satisfied. The pitch angles of the Toyota Yaris had similar trend to those of the test vehicle except for those within the first 0.1 seconds. The roll angles of the Toyota Yaris also had a similar trend to those of the test vehicle for the most part of the impact except for the time when the Yaris started impacting the barrier. The discrepancies of pitch and roll angles between simulation results and test data could be caused by the structural differences of the two vehicles, even though both were MASH compliant. Nevertheless, the overall trends of yaw, pitch and roll angles of the vehicle in the simulation were similar to those of the test vehicle. The pitch and roll angles of the Toyota Yaris were less than 75°, which satisfied the requirement of MASH criterion *F*. The occupant risk factors, i.e., OIVs and ORAs, were found below the MASH limit values; therefore, the MASH criterion *H* was satisfied. For the occupant risk factors, the largest discrepancy between simulation results and actual test data was observed on the ORA in the longitudinal direction, which had a 36.7% relative error. It should be noted that there was no specified limit in MASH for the maximum allowable difference between simulation

results and test data for the occupant risk factors. In NCHRP Report W179, it was suggested that the difference between FEA results and test data for each occupant risk factor be less than 20 percent unless the magnitude was relatively small. Since the magnitudes of the ORAs and OIVs were relatively small in the above-mentioned case of this study, the simulation results were considered acceptable based on the limit values given in NCHRP Report W179. Overall, the MASH evaluation criteria *A*, *D*, *F*, and *H* were satisfied.

The acceleration, velocity and displacement profiles of the 2007 Chevy Silverado were similar to the actual test data. The vehicle was safety contained and redirected, thus satisfying MASH evaluation criterion *A*. The examination of debris and vehicle deformation from the simulation results indicated that MASH evaluation criteria *D* was satisfied. The roll and yaw angles of the 2007 Chevy Silverado throughout the impact had similar trend as the test data. The pitch angles of the Chevy Silverado had similar trend to those of the test vehicle except for those within the first 0.1 seconds. The discrepancies of roll angles between simulation results and test data could be caused by the structural differences of the two vehicles, even though both were MASH compliant. The pitch and roll angles of the 2007 Chevy Silverado were less than 75°, which satisfied the requirement of MASH criterion *F*. All the OIVs and ORAs were below the MASH limit values; therefore, the MASH criterion *H* was satisfied. The largest discrepancy between the actual test and simulation's occupant risk factors was observed on the OIV in longitudinal direction, which had a 25.3% relative error. Since the magnitudes of the ORAs and OIVs were relatively small, the simulation results were considered acceptable based on the limit

values given in NCHRP Report W179. Overall, the MASH evaluation criteria *A*, *D*, *F*, and *H* were satisfied.

The simulation results showed that the acceleration, velocity and displacement profiles of the 2014 Chevy Silverado were similar to the actual test data. The vehicle was safety contained and redirected, thus satisfying MASH evaluation criterion *A*. The examination of debris and vehicle deformation from the simulation results indicated that MASH evaluation criteria *D* was satisfied. The roll and yaw angles of the 2014 Chevy Silverado throughout the impact had similar trend as the test data. The yaw, pitch and roll angles of the 2014 Chevy Silverado throughout the impact had similar trend as the test data. The pitch and roll angles of the 2014 Chevy Silverado were less than 75°, which satisfied the requirement of MASH criterion *F*. All the OIVs and ORAs were below the MASH limit values; therefore, the MASH criterion *H* was satisfied. The largest discrepancy between the actual test and simulation's occupant risk factors was observed on the OIV in longitudinal direction, which had a 34.5% relative error. Since the magnitudes of the ORAs and OIVs were relatively small, the simulation results were considered acceptable based on the limit values given in NCHRP Report W179. Overall, the MASH evaluation criteria *A*, *D*, *F*, and *H* were satisfied.

Despite the discrepancy between simulation results and the test data, finite element analysis was shown to be a viable means for crash analysis of roadside safety structures in this study. Future research can be conducted to improve the material model with failure and damage mechanism for the vehicle's hood so as to accurately simulate the tearing of the hood that was observed in the actual crash test using a 2015 Chevy Silverado. Another area of future research is to investigate how the effects of static and dynamic frictions on

the vehicular responses in the FE simulation. As for the two-bar bridge rail design, future work can be conducted to determine the optimum spacing between the top and bottom rails that would cause minimum hood tearing or potential snagging of the vehicle under the rails.

REFERENCES

Barker, R. M., & Puckett, J. A. (1987). *Design of highway bridges based on AASHTO LRFD bridge design specifications*.

Nordlin, E. R., Field, R. N., & Hackett, R. P. (1965). Dynamic Full-Scale Impact Tests of Bridge Barrier Rails. *Highway Research Record*, (83).

Nordlin, E. F., Hackett, R. P., & Folsom, J. J. (1970). Dynamic Tests of California Type 9 Bridge Barrier Rail and Type 8 Bridge Approach Guardrail. *ESTADOS UNIDOS. Highway Research Record. Bridges, foundations, and retaining walls. Washington, DC*.

Michie, J. D. (1981). *Recommended procedures for the safety performance evaluation of highway appurtenances* (No. HS-032 597).

Horne, D. A. (1997). ACTION: Crash Testing of Bridge Railings FHWA Memorandum.

NCDOT. (2017). Roadside Safety Hardware – MASH-16 Implementation Plan. *State of North Carolina Department of Transporation.*

Issacson, L. (1986). Federal highway program and wetland mitigation. *Proceedings: Mitigation of Impacts and Losses (Jon Kusler, ed.). Association of State Wetland Managers. Berne, NY*.

Ross Jr, H. E., Sicking, D. L., Zimmer, R. A., & Michie, J. D. (1993). *Recommended procedures for the safety performance evaluation of highway features* (No. 350).

Weintrob, L. H. (1997). *Management advisory memorandum on relocation of utilities, Central Artery/Third Harbor Tunnel, FHWA region 1: memorandum*. US Dept. of Transportation, Office of Inspector General.

Faller, R. K., Ritter, M. A., Rosson, B. T., Fowler, M. D., & Duwadi, S. R. (2000). Two test level 4 bridge railing and transition systems for transverse timber deck bridges. *Transportation research record*, *1696*(1), 334-351.

Rails, A. B., Bullard Jr, D. L., Williams, W. F., Menges, W. L., & Haug, R. R. (2002). Design and Evaluation of the TXDOT F411 and T77.

Williams, W. (2008). New Aesthetic Type T-1F Bridge Rail from the Texas Department of Transportation: Design and Test Level 3 Crash Testing. *Transportation research record*, *2050*(1), 39-46.

Meline, R., Jewell, J., & Peter, R. (1999). *Vehicle crash tests of the type 80 bridge rail* (No. FHWA/CA/ESC-98/06 Part 3,).

Whitesel, D., & Jewell, J. R. (2008). *Development and crash testing of an aesthetic, see-through bridge rail, type 90*. State of California Department of Transportation, Division of Research and Innovation, Office of Safety Innovation and Cooperative Research.

AASHTO, M. (2009). Manual for assessing safety hardware (MASH). *Washington, DC*.

Rentz, H. H. (1998). National Cooperative Highway Research Program (NCHRP) Report 350 Hardware Compliance Dates. *FHWA Memoradum*.

Ross Jr, H., Sicking, D., Zimmer, R. A., & Michie, J. D. (1993). *Recommended procedures for the safety performance evaluation of highway features*.

Williams, W. F., & Holt, J. (2013). *Design and Full-Scale Testing of Texas Department of Transportation Type T131RC Bridge Rail* (No. 13-4675).

Williams, W. F., Bligh, R., Odell, W., Smith, A., & Holt, J. (2015). Design and Full-Scale Testing of Low-Cost Texas Department of Transportation Type T631 Bridge Rail for MASH Test Level 2 and 3 Applications. *Transportation Research Record*, *2521*(1), 117-127.

Whitesel, D., Jewell, J., & Meline, R. (2015). *Compliance Crash Testing of the Caltrans Type 26 Bridge Rail* (No. CA15-2181).

Feinsod, S., Urroz, E. R., Haas, P., & Griffith, J. (2016). *Compliance Crash Testing of the Type 732SW Bridge Rail* (No. CA16-2637).

AASHTO. (2014). AASHTO LRFD Bridge Design Specifications, Customary U.S. Units, 7th Edition, with 2015 and 2016 Interim Revisions. *American Association of State Highway and Transportation Officials.*

AASHTO. (2016). Manual for Assessing Safety Hardware (MASH-2) - 2nd Edition. *American Association of State Highway and Transportation Officials (AASHTO). Washington, D.C.*

Wright Jr, F. G. (2000). Bridge Rail Analysis *FHWA Memoradum.*

Barker, R. M., & Puckett, J. A. (2013). Design of Highway Bridges - An LRFD Approach. *John Wiley & Sons.*

Wekezer, J. W., Oskard, M. S., Logan, R. W., & Zywicz, E. (1993). Vehicle impact simulation. *Journal of transportation engineering*, *119*(4), 598-617.

Mendis, K., Mani, A., & Shyu, S. C. (1995). *Finite element crash models of motor vehicles* (No. FHWA-RD-016). United States. Federal Highway Administration.

Cofie, E. (1995). *Finite element model of a small automobile impacting a rigid pole*. Federal Highway Administration, Turner-Fairbank Highway Research Center.

Zaouk, A. K., Bedewi, N. E., Kan, C. D., & Marzougui, D. (1997). Development and evaluation of a C-1500 pick-up truck model for roadside hardware impact simulation.

Ray, M. H., Oldani, E., & Plaxico, C. A. (2004). Design and analysis of an aluminum F-shape bridge railing. *International Journal of Crashworthiness*, *9*(4), 349-363.

Williams, W. (2008). New Aesthetic Type T-1F Bridge Rail from the Texas Department of Transportation: Design and Test Level 3 Crash Testing. *Transportation research record*, *2050*(1), 39-46.

Mohan, P., Marzougui, D., Arispe, E., & Story, C. (2009[a]). Component and full-scale tests of the 2007 Chevrolet Silverado Suspension System. *NCAC Test Report*.

Mohan, P., Marzougui, D., Arispe, E., & Story, C. (2009[b]). Component and full-scale tests of the 2007 Chevrolet Silverado Suspension System. *NCAC Test Report*.

Fang, H., Weggel, D. C., Bi, J., & Martin, M. E. (2009). *Finite Element Evaluation of Two Retrofit Options to Enhance the Performance of Cable Media Barriers* (No. FHWA/NC/2008-10). North Carolina. Dept. of Transportation. Research and Analysis Group.

Marzougui, D., Samaha, R. R., Cui, C., Kan, C., & Opiela, K. S. (2012). Extended validation of the finite element model for the 2010 Toyota Yaris Passenger Sedan. *National Crash Analysis Center, George Washington University, Washington, DC, Report No. NCAC*.

Abu-Odeh, A. (2008, June). Modeling and simulation of bogie impacts on concrete bridge rails using LS-DYNA. In *10th international LS-DYNA Users Conference, Livermore Software Technology Corporations, June* (pp. 8-10).

Murray, Y. D., Abu-Odeh, A., & Bligh, R. (2007). Evaluation of concrete material model 159. *Rep. No. FHWA-HRT-05, 63*.

Schwer, L. (2014, June). Modeling rebar: The forgotten sister in reinforced concrete modeling. In *13th International LS-DYNA® Users Conference*.

Narkhede, S., Lokhande, N., Gangani, B., & Gadekar, G. (2010). Bolted joint representation in LS-DYNA® to model bolt pre-stress and bolt failure characteristics in crash simulations. In *11th International LS-DYNA® Users Conference.*

Hadjioannou, M., Stevens, D., & Barsotti, M. (2016). Development and Validation of Bolted Connection Modeling in LS-DYNA® for Large Vehicle Models. In *14th International LS-DYNA Users Conference.*

Younger, P. L., & Adams, R. (1999). Predicting Mine Water Rebound: R&D Technical Report W179. *Environment Agency, UK*.